DELINEATING AND INTERPRETING THE GOLD (MINERALISATION) VEINS AROUND BIDA AND ZUNGERU AREA OF NIGER STATE, NIGERIA USING AEROMAGNETIC AND RADIOMETRIC DATA

BY

ALIYU, Shakirat Bukola
(MTech/SPS/2017/7030)

DEPARTMENT OF PHYSICS
SCHOOL OF PHYSICAL SCIENCES
FEDERAL UNIVERSITY OF TECHNOLOGY, MINNA.

SEPTEMBER, 2021

DELINEATING AND INTERPRETING THE GOLD (MINERALISATION) VEINS AROUND BIDA AND ZUNGERU AREA OF NIGER STATE, NIGERIA USING AEROMAGNETIC AND RADIOMETRIC DATA

BY

ALIYU, Shakirat Bukola
(MTech/SPS/2017/7030)

A THESIS SUBMITTED TO THE POSTGRADUATE SCHOOL, FEDERAL UNIVERSITY OF TECHNOLOGY, MINNA, NIGERIA IN PARTIAL FULFILLMENT OF THE REQUIREMENTS FOR THE AWARD OF THE DEGREE OF MASTER OF TECHNOLOGY IN APPLIED GEOPHYSICS

SEPTEMBER, 2021

ABSTRACT

Both Airborne Magnetic and Radiometric dataset were employed to interpret the geology and geological structures that serve as host to gold and other solid minerals within the Bida (Sheet 184) and Zungeru (sheet 163). An area of 55 by 110 km square is contained within the cretaceous sediments of Bida Basin and the meta-sediments of Zungeru-Sarkin-Pawa schist belt. Data interpretation adopted concentrated on mapping geological structures, boundaries and possible gold mineralisation veins that arises from hydrothermal altered zones. Application of mathematical algorithm for data enhancing such as, Reduce-to-the-Equator and Analytical signal, to the magnetic data, Potassium (K), Thorium (Th), Uranium (U) and Ternary image of the radiometric data helps in delineating the NW-SE trending contact separating the cretaceous sedimentary formation from the meta-sediments. This trend takes off from the Southern end Bida and terminates at the Western end of Bida. The first vertical derivative and the CET analysis help in mapping the fractures, folds and contact zones. Majority of the structures delineated exist around the meta-sediments. Primarily at the Northern end of the study area are linear faults and fractures trending NE-SW around Zungeru – Yakila – Katako axis and ranges from 2 to 5 km in length within mylonite formation. Also, below Federal University of Technology Minna main campus around Minkwogi, Sunbwagi, Sabon-Dagga, Kakagi and Bobo Shiri area, are chunk of interconnected short fracture zones that exist within the magmatite. Belt type meta-sediment complexes. Results from the Analytical signal, vertical derivative, Eular Deconvolution and CET-plugin showed that most of these structures and their depth were located with in northern part and south-western region of the study area. The coordinate of these major structures and lineaments that shows degree of mineralisation were mapped on CET map most interestingly is between longitude 6˚20E to 6˚30E and latitude 9˚10N to 9˚30N. Where the meta-sediments have been intruded by medium to coarse grain biolite granite, is an evidence of structural control veins, which coincided with regions of hydrothermally, altered zones on the ternary map.

TABLE OF CONTENTS

CHAPTER THREE

CHAPTER FOUR

LIST OF TABLES

LIST OF FIGURES

CHAPTER ONE

1.0 INTRODUCTION

1.1 Background to the Study

Mineral is a naturally occurring inorganic element or compound having an orderly internal structure and characteristic chemical composition, crystal form, and physical properties. Common minerals include quartz, feldspar, mica, amphibole, olivine and calcite. The physical properties of minerals such as their hardness, lustre, color, cleavage, fracture and relative density can be used to identify minerals. These general characteristics are controlled mainly by their atomic structure crystal (HKGS, 2009). In geology and mineralogy, the term "mineral" is usually reserved for mineral species, crystalline compounds with a fairly well-defined chemical composition and a specific crystal structure. Mineral without a definite crystalline structure such as opal or obsidian are then more properly called mineraloids. If a chemical compound may occur naturally with different crystal structures each structure is considered different mineral species example quartz and stishovite are two different minerals consisting of the same compound silicon dioxide. Minerals being natural chemicals are classified according to their chemistry and crystal form. A basic classification for minerals is native element are gold, silver, mercury, granite, diamond. Oxides (Corundum, hematite, spine) Sulfides (pyrite, galena), Hydroxides (Goethite, brucite) Carbonates (calcite, magnesite, dolomite) Sheet silicates (Muscovite mica, biotite mica, clay minerals) Framework silicates (quartz, feldspar).

Silicate minerals are the most abundant components of rocks on the earth's surface, making up over 90 percent by mass of the earth's crust. The fundamental chemical building block of silicate minerals is the chemical compound silicon tetra oxide

SiO_4. (HKGS, 2009). Rocks are made of mineral element; element are simple substances that cannot be broken down into any other substance. Only a few minerals are rock forming and most rock is made from a combination of the component of these such as feldspars, quartz, mica, olivine, calcite, pyroxene, and amphiboles. Most other minerals of which there are over 3000 different types are rarely present in a quantity that is large enough to be considered as rock forming. To consider a common rock forming mineral must be one of the most rock abundant mineral in the earth crust, be one of the original minerals presents at the time of a crustal rock formation and an important mineral in determining a rock's classification (Hobart, 2005).

Potassium (K) is a building block of some of the most widespread minerals but despite that, it is actually surprisingly rare in the whole Earth. It can be even said that potassium is a trace element. It forms only 160 ppm (0.16%) of the bulk earth. It is an important constituent of k-feldspar and mica and these are among the major component of granitic. Granite rhyolite, stale, shale, arkoses and so on, are the common rock and potassium is abundant there and found abundant in the upper continental crust. It belongs to the alkali metals group. Other geological significant metals in this group are sodium and lithium. These elements are very reactive because they contain only one outermost electron. They are therefore always on the lookout for the potential partners. We will never find uncombined potassium in nature because of that potassium tends to form ionic compound. Potassium and sodium are very similar to other chemically and their behavior in geological materials in analogous as well (Mittlefehldt and David, 1999).

Radioactive decay is an important source of earth's internal heat, because the concentration of potassium is so much higher in the continental crust than in the mantle. The geothermal gradient and heat production is also higher there. It is not the only heat

producing element but other heat producers such as uranium and thorium are also highly incompatible in the mantle and therefore gather in the continental crust just as potassium does. Potassium readily dissolves in water during weathering of potassium-bearing minerals and enters the hydrosphere for a long time. It goes relatively easily into the water, but it is not easy to take it back. All it takes is to vaporise the water until potassium precipitates out of its as evaporate mineral sylvite (KCL), but very high rate of evaporation is needed for it to occur. Therefore, potassium tends to stay in the hydrosphere for a long time (Mittlefehldt and David, 1999).

This work focuses on the analysis and interpretation of the aeromagnetic and radiometry data over some parts of Niger State (Minna and part of Central Bida Basin). The outcome of the analysis is expected to throw more light on the geological features, minerals and other linear features as related to the mineralisation potential of the study area.

1.2 Statement of the Research Problem

In line with the current trend in Federal Government policy which is encouraging state governments agencies and parastatals to find means of improving on their internally generated revenue fund (IGRF), rather than relying on Government funding. This prompts the authorities of the Federal University of Technology Minna to look into the possibility of exploring the solid mineral (especially gold) potentials that are located within his neighborhood so as to generate more funds (FUTMinna Book of Speeches, 28th Convocation Ceremony). This idea is not out of place as the University is situated within the contact/boundary between the Bida sedimentary basin and the Zungeru/ Sarkin-Pawa Schist belt. These regions are marked by several volcanic activities which give rise to the structures that serve as host to this mineral.

1.3 Justification of the Study

Both aeromagnetic and radiometric methods are very effective in environmental monitoring and geological mapping. The result from radiometric and aeromagnetic survey will delineate the geology structure like fault, fold, basement structure for mineral which are possible host, target and assist in locating some intrusive body related to mineral deposits and its magnitude. The outcome of this research will provide solution to address where exactly the mineral of interest is located and also their depth so occurrence. Exploring these minerals would in no doubt increase the internally generated revenue of the University.

1.4 Aim and Objectives of the Study

The aim of this project is to delineate delineating and interpreting the gold (mineralisation) veins around Bida and Zungeru area of Niger State, Nigeria using aeromagnetic and radiometric data.

The objectives are to;

i. Interpret the Total Magnetic Intensity (TMI) of the area to indicate regions of high and low magnetic susceptibilities.
ii. Obtain the horizontal derivatives, analytical signal, vertical derivative and Central Exploration Targeting (CET) in order to position anomalies directly above the causative body, delineate both deeper and shallow structures that could be faults, fracture, intrusive bodies, lineament that are veins.
iii. Produce ternary map by combining the data of Potassium K (in red), Thorium Th (in green) and Uranium U (in blue) to map geology contact, while correlate with Geology map of the study area and delineate the regions of highs and lows for the three (3) elements namely Potassium, Thorium and Uranium

iv. correlate the structure obtain from the magnetic field with that of the radiometric interpretation to delineate the mineralisation zone.

CHAPTER TWO

2.0 LITERATURE REVIEW

2.1 Review of Geological work of the Area

Niger State lie between latitudes 8°15 – 11°5´N and longitudes 4°00-7°15´E. It is bordered in the North with the North Kaduna and Kebbi States and in the South by Kogi State. It shares boundary in the west with Kwara State and Benin republic and in the east with Federal Capital territory and Kaduna State as shown in the geology map of Nigeria (Figure 2.1). Niger State is divided into twenty-five local governments with landmass of about 80,000 square kilometers. The Minna area comprises of Meta sedimentary and meta-igneous rocks which have undergone polyphase deformation and Metamorphism (Alabi, 2011). The study area is located within Bida and Zungeru, bounded by the longitude 6°00´E and 6°30´E and latitude 9°00´N and 10°00´N as show in figure 2.2, it occupies the mid-Niger of the Bida basin. These rocks have been intruded by granitic rocks of Pan-African age. Five litho stratigraphic units have been recognised in Minna area. The schist which occur as a flat laying narrow southwest-northeast belt at the central part of Minna with small quartzite ridge parallel to it, the gneiss occurs as a small suite at the northern and southern part of the area forming a contact with the granite. Feldspathic rich pegmatite is bounded to the east, with average width of 65 meters and 100 meters long, the pegmatite host tourmaline. Granitic rocks dominate the rock types in the area and vary in texture and composition. Detailed geological mapping of the area was carried out on a map scale 1: 25,000 using geological compass clinometers, hammer and GPS (Alabi, 2011).

In 1966, Buser established existence of paleo structures which have direct activities like tectonic movements, metamorphism, mineralization and drainage. In this regards a great

contribution was made by Ajakaiye *et al.* (1991) which interpreting aeromagnetic data across the Nigeria continental mass, they identified that NE-SW trending anomalies are the dominant magnetic fractures of most of this area. Similarly, Udensi *et al*. (2003) added a new dimension to the studies, he applied both qualitative and quantitative approaches and established trend and the structural patterns within the Bida basin from aeromagnetic data. They observed that the northern part (Upper part) of the Bida basin is dominated by NE-SW trend. The central part by E-W trend, while the southern part is dominated by ENE-WSW trends. Also, the Precambrian basement complex of Nigerian as an integral part of West African craton is known to have been subjected to various episode of deformation. These activities show the presence of geological structures like fold, foliations and fractures of varying magnitude. Hubbard (1975) recognised one of such as a mega-structure in the Ife Wara - Zungeru fault which extends in the western and northern parts of Nigeria.

Alabi, (2011) also detected eight large granitic masses occurring as batholiths and continuous uninterrupted ridge in northeast direction of about 18 km long, average width of 1.5 km and an average height of 35 meters above their surrounding plains such granitic batholiths occur as Paiko and Minna batholiths.

Idris *et al.* (2015) Carried out groundwater development in a mixed geological terrain in Niger State and discovered that groundwater occurrence in Niger State is controlled by the prevailing climate factors and geology. Areas underlain the Basement Complex rocks have greater groundwater potential when deeply weathered or fractured. Depth and intensity of weathering varies widely in the area and range from 2 m to 30 m, the weathered product mostly comprises of sand and clay with the former having a higher percentage.

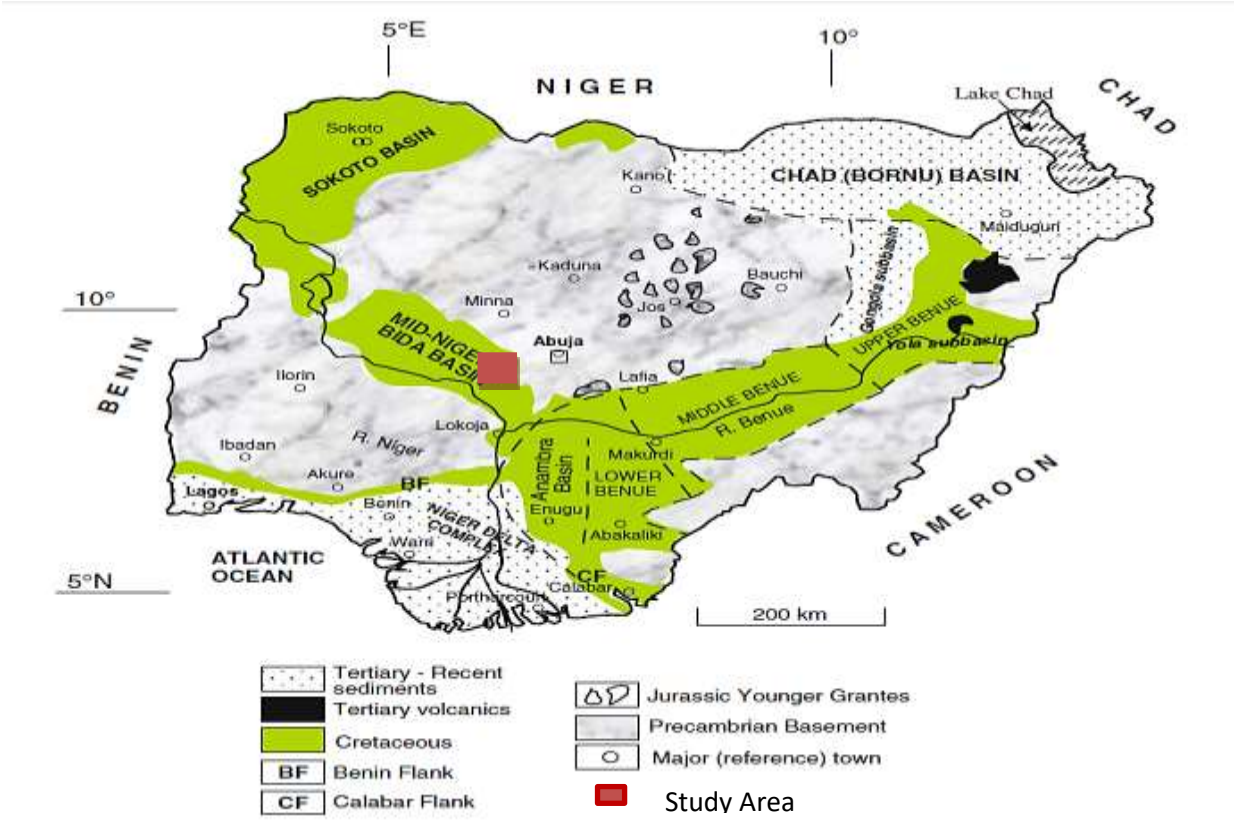

Figure 2.1**:** Geology map of Nigeria showing the major geological components, basement, younger granites and sedimentary basin (After Obaje, 2009).

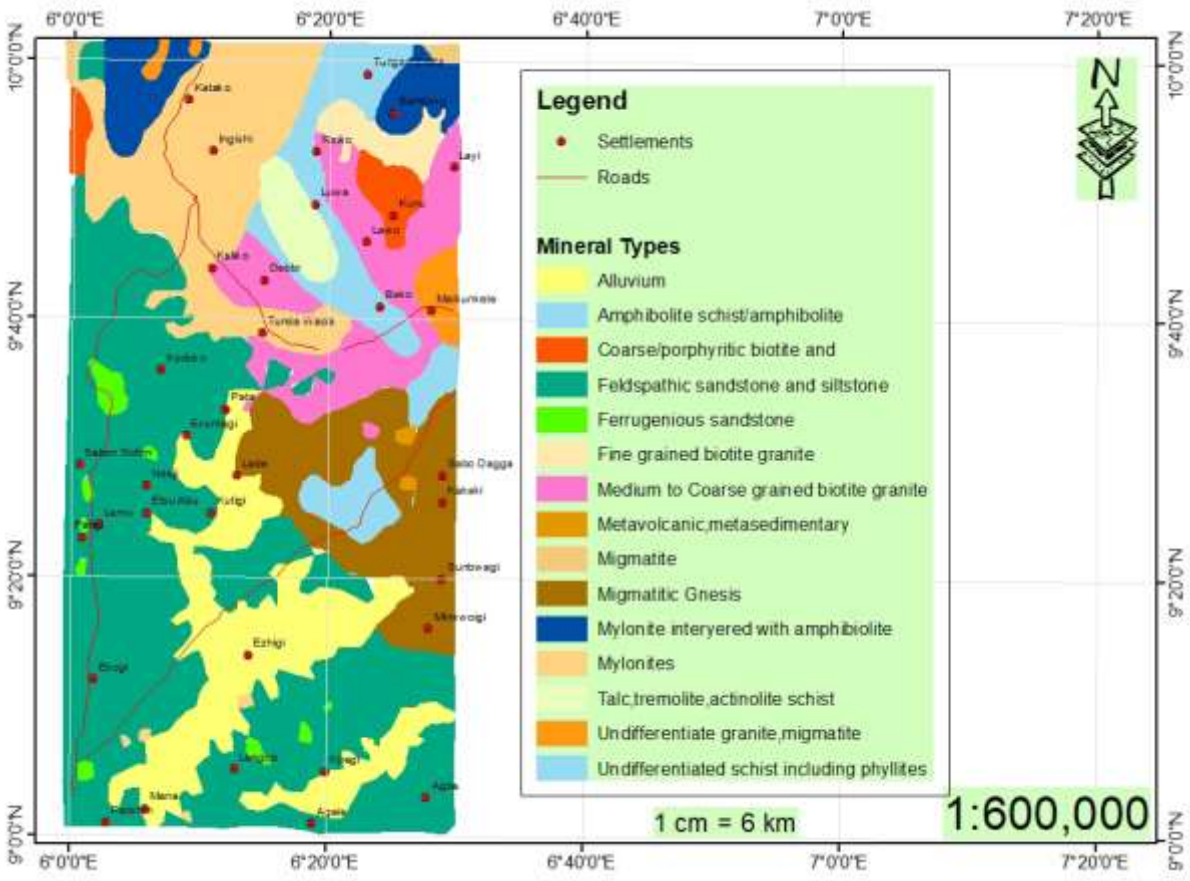

Figure 2.2: Geology map of the study area (Modified from NGSA, 2009)

2.2 Geophysical Review of the Study

Bello (2012) also used electrical resistivity technique to delineate gold deposit site in Minna, he discovered that there are injections of deposits that is haloes of deposited are distributed over the site. The nature of soil is alluvial and has an average depth of 5-6 meter from the surface, also discovered that gold is strongly dispersed by chemical and mechanical processes resulting in haloes that could extend several kilometers, he also suggested that other geophysical techniques should be used as a comparative technique.

Nwugha *et al.* (2012) determine the depth to some anomalous within Angba, Ankpa and Oturkpa in lower Benue trough, using suffer 8 software to filtering data and contour it in order to produce magnetic identifiable anomalies low and highs. In their finding they obtained 6.72 ± 0.58 km for maximum depths between Oturkpa and Ogbadibu town and

1.09km ± 0.58km for minimum depths with the used of peter's maximum slope method. Also explained that the sequence of closed lows east Oturkpa is due to largest part of an irregular metamorphic basement, that has been occupied with sediments or faulted metamorphic occupied with sediments. He discovered that there is fault around Ogbadibu and Imane as well as Oturkpo area with signs of 333 discontinuous lineation and circular to cylindrical anomalies.

Adetona and Mallam (2013) also obtained sedimentary thickness over the lower Benue trough within study area to be approximately 10 km and it was observed that the prevalence of magnetic lows within the modeled residual field data show acidic basement (deformed granitic basement). The source parameter imaging revealed a minimum depth of 76.983 meters and a maximum sedimentation thickness of 9.847 km, which also occur within Idah, Ankpa, and Udegi axis. The depth estimated by this research particularly around the Anambra basin underneath Idah and Angba in Kogi state is of significance interest, because it is high enough for the realization of temperatures approximately 60 ºC and higher than is essential for thermal degradation of kerogen yielding hydrocarbons.

David and Marius (2013) also interpret the aeromagnetic data over some parts of lower Benue trough using spectral analysis techniques, and four aeromagnetic data sheets of $1/2^0 \times 1/2^0$ on the scale of 1:100,000 covering some parts of lower Benue trough was used to determine the mean depth values of magnetic sources. The result obtained shows a two - layered source model, with the deeper magnetic source located at depths varying between 1.6 km and 6.13 km with a mean value depth of 3.03 km. This represents the magnetic basement surface and the depth to the shallower magnetic source was found to vary from 0.06 km to 0.37 km with the mean value depth of 0.22 km indicating the presence of magnetic intrusive bodies within the basement.

John *et al*. (2013) employed the analysis of aeromagnetic and radiometric data in the assessment of geothermal and radioactive heat emanating from southern part of Bida basin, Nigeria. The research covered both basin and basement rock sections and was aimed at determining the geothermal heat flow and radioactive heat characteristics of the survey area. The research results revealed a geothermal heat flow values to be range 69.167 $mW\,m^{-2}$ to 124.821 $mW\,m^{-2}$ with an average value of 90.959 $mW\,m^{-2}$ and radioactive heat values ranging from 0.91 to 4.53 $\mu W\,m^{-2}$ with an average value of 2.28 $\mu W\,m^{-2}$. He concludes that the katakwa part of the study area as a prospect area for geothermal heat.

John *et al.* (2013) employed the analysis of aeromagnetic data for lineament study over parts of southern Bida basin, Nigeria. This research revealed that the mineralisation pattern of the survey area is structurally controlled. Several magnetic lineaments were deduced from the study, and the predominant trends of the lineaments are east-west, north-south, northeast-southwest and northwest-southeast directions. The northwest-southeast trends reflect the younger tectonic events, because the younger events are more pronounced and tend to obliterate the older events, thus it may indicate recent faulting of country rock. In addition, it is inferred that the northeast-southwest trending Romanche Fracture Zone passed through the survey area.

Nwosu (2014) determine the depth to the magnetic basement over some parts of middle Benue trough using source parameter imaging (SPI). The result shown two main magnetic anomaly sources depth namely deep magnetic bodies lying with thick sedimentary formations ranges from 2000 to 6291.5 m with a mean average depth of 3245 m signifying the magnetic basement depth.

Ngama and Akanbi (2017) also did qualitative interpretation on aeromagnetic data of Naraguta area, north central and reveal the variation in the magnetization of the magnetic source in the study area using analytical signal method. It has amplitude range of between 0.000 nT/m to 3.555 nT/m and observed high peaks in the parts of Ropp, herpangmiamgo and Rukuba complex. Analytical signal maximum represents the edges of circular, elliptical or polygonal porphyritic ring dykes that characterize many of the complexes in the study area.

Jude *et al.* (2017) Used aeromagnetic data coupled with Landsat ETM + data and SRTM DEM to map regional hydro geological structures in the basement complex region of Paiko. The result showed that the lithologic units comprised alluvial deposits, granite, gnesis and magmatite. The alluvial deposit occupied streambeds and stream banks composed of sand, silt and clay in various proportions with some pebbles and cobbles with colouration from grayish white through reddish brown to black. There is a variation in the height of the outcrops which range from steep hills to low lying massive stock with gentle elevations and textures ranging from fine to coarse. Magmatites, which are the most widespread lithology within the study area, are low lying. Gneisses occur as a group of minor discontinues intrusions of small area extent in the migmatities. Granitic rocks mainly as high, extensive whalebacks. They form the highest elevation in the area. Foliations in gneisses gave dominant trend of NW-SE and NE-SW. Transcurrent faults sets were observed in the area. Fault axes of 40˚- 60˚ were measured in the granites. The principal joint directions trend NW-SE, and minor joint directions trend NW-SW.

Oke *et al*. (2018) Conducted spectral analysis, source parameter imaging and Euler depth determination method over part of Bida Basin. Revealed maximum depth of 3.56 km around Mokwa and Batati areas. Shallow source also exists around Pategi, Paiko, Izom

and Lapai area with an average depth ranging from 107.74 m to about 514.82 m. Source parameter imaging shows a deeper sedimentary thickness of 4.2 km in the same area with Euler deconvolution. Spectral depth analysis also showed a maximum sedimentary thickness of 3.50 km.

CHAPTER THREE

3.0 MATERIALS AND METHOD

3.1 Location of the Study Area

The study area is located within the Bida (184) and Zungeru (163) sheets in Niger State, bounded by the longitude 6°00´E and 6°30´E and latitude 9°00´N and 10°00´N as show in Figure 1.1. This study area experience distinct dry and wet seasons with annual rain fall varying from 1,100mm in the northern parts to 1,600mm in the southern parts. The maximum temperature is recorded between March and June, while the minimum is usually between December and January. The rainy seasons last for about 150 days in the northern parts to about 120 days in the southern parts of the State. It occupies an area of 110 by 55 km starting from Bida sedimentary basin extending into the Zungeru metasediments.

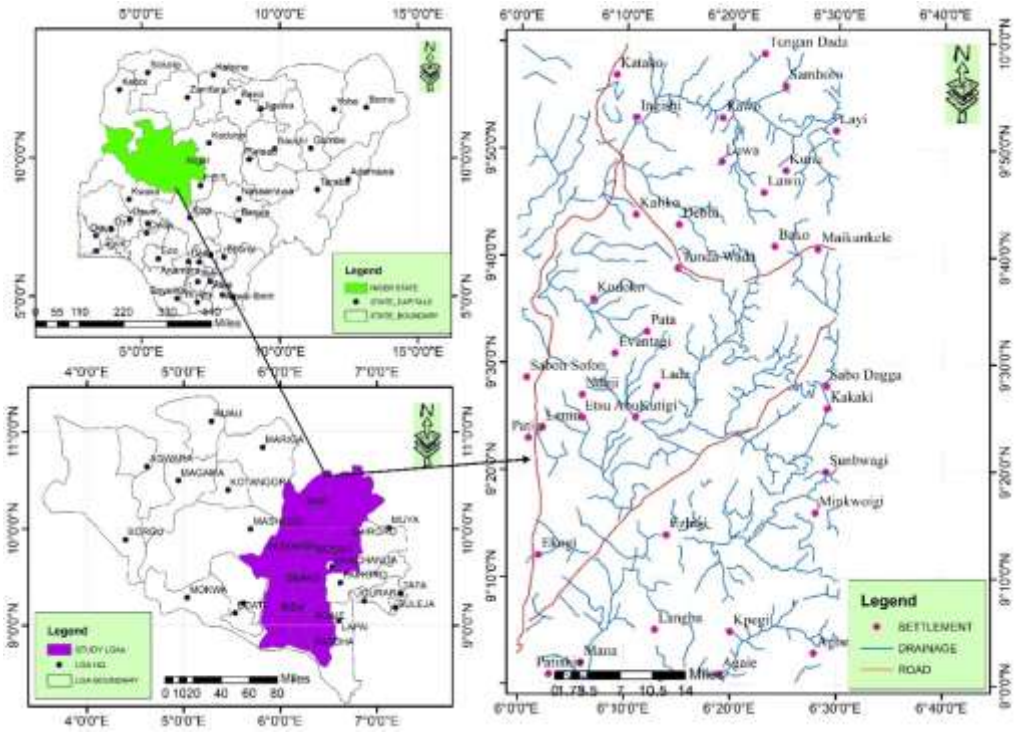

Figure 3.1: Location map of the study area (Modified from Administrative map of Nigeria)

3.2 Materials

The total field magnetic data and radiometric data of Bida and Zugeru area were acquired from the Nigeria Geology Survey Agency. The geomagnetic gradient was subtracted from the map using IGRF. The research work made use of Oasis Montaj software in the production of the total magnetic intensity (TMI) map and Ternary Map which were further subjected to different method for analyses.

The materials to be used for this project include:

i. Aeromagnetic data covering the study area (Bida and Zungeru sheets)
ii. Radiometric data (Potassium, Thorium and Uranium)
iii. Geology map
iv. Geosoft (Oasis Montaj Software)
v. MatLab
vi. Microsoft Excel
vii. Computer
viii. Stationeries (paper, pen, pin, ruler etc.)

3.3 Method

The procedure adopted in this research work includes:

I. Production of composite aeromagnetic map of the study area
II. Application of reduction to equator to remove the dependence of the data on angle of inclination and declination.
III. Obtaining the horizontal derivative in order to enhance near surface structures and produce input data for further analysis.

IV. Computing the vertical and tilt derivative to mapped lineaments and geological contact respectively

V. Evaluating the analytical signal so as to delineate region of out crop near surface intrusive bodies and equally to place the anomaly directly above the causative body.

VI. Evaluating the Centre for Exploration Targeting (CET) to map basement and superficial lineaments

VII. Evaluating the Euler Deconvolution to obtain depth to magnetic source.

VIII. Correlating the structures from 1VD, Central Exploration Targeting (CET) and Geology map.

IX. Analysis of Potassium K, Thorium Th and Uranium U Concentration maps to delineate the regions of highs and lows concentration

X. Production of radiometric ratio of K/U, Th/U, Th/K and U/K in maps and relate them to delineated veins.

XI. Production of ternary map to map geological boundaries and correlate with Geological map

XII. Delineation of solid mineral zone within the study area through the structures identifies.

3.4 Data Acquisition

Two aeromagnetic maps and two Aeroradiometric maps each of K, Th and U sheet were acquired from the Nigeria Geological Survey Agency covering the study area bounded by longitude 6º00 to 6.5º0E and latitude 9º00 to 10º00N. The surveys were carried out in two phases, phase I, was entirely financed by the Government of Nigeria. The data acquisition, processing and compilation were done by Fugro airborne surveys which was

completed in September 2007 and it included 826,000-line kilometers of magnetic and radiometric surveys flown at 500 m profile spacing, 2 kilometers tie-line spacing and 80 m terrain clearance.

As part of a major project known as the sustainable management for mineral resource project by Word Bank of Nigeria supported the phase II, surveyed blocks which were not covered in phase I completed in August 2009. It included 1,104,000-line kilometers of magnetic and radiometric surveys flown at 500 m line spacing and 80 m terrain clearance.

3.5 The International Geomagnetic Reference Field (IGRF)

It should be noted that the scope of aeromagnetic surveys is to record the variations in F with x and y over a survey area while removing all time-based variations. Between 20000 and 70000 nT will be the magnitude of F everywhere on earth and it expected to have local variations of several hundred nT due to the effects of the magnetization of the crustal geology. The 'anomalies' are always at least two sequence of magnitude smaller than the value of the total field. Subtracting on a rational basis and the expected variation in the main field to leave anomalies that may be compared from one Survey to another are provided by IGRF. Since IGRF removal implies the subtraction of about 99% of the measured Value, the IGRF needs to be defined with precision if the remainder is to keep accuracy and credibility. (Clark and Emerson 1991).

3.6 Theory of Magnetic and Aeromagnetic

Magnetism refers to physical process arising from the force between magnets, objects that generate fields that attract or repel other objects. All materials experience magnetism, some are stronger than others. Permanent magnets, made from materials such as iron, experience the strongest effects, known as ferromagnetism. This is the only form of

magnetism strong enough to be felt by people. Then there's Para magnetism, in which materials are attracted by a magnetic field, and diamagnetism, in which materials are repelled by a magnetic field. Other, more complex forms such as anti-ferromagnetic, in which the magnetic properties of atoms align next to each other; and spin glass behavior, which experience both ferromagnetic and anti-ferromagnetic interactions. Some materials are called non-magnetic, because their magnetic effects are too small. Magnetism also enables certain materials to attract or repel each other. It is used in aircraft in applications as the compass, alternators generators, starter motors, relays, navigation and instruments. It also a material consists of small particles each having a south and a north pole and they are all aligned in one direction. Non magnetized materials have exactly the same particles. The only difference is that they are not aligned at all but they are in a totally random chaotic order. In the area around a magnet be a magnetic field and this was proven by a compass. This magnetic field is called flux. Some materials are magnetized without much difficulty; they also lose their property with the same ease. Soft iron is one of example, and this makes it suitable to use for temporary magnets. Other materials are not so easily magnetized e.g. iron, steel but when they are magnetised they will not lose that property so easily. This is why they used as permanent magnet. You will need to heat them in order for them loose their permanent magnetic field.

This is types of geophysical survey carried out using a magnetometer aboard or towed behind an aircraft. The principle is the same with magnetic survey carried out with hand-held magnetometer but it gives room for much large areas of the earth’s surface to be covered on time for regional reconnaissance. The flies of the aircraft are typically in a grid-like pattern with height and line spacing determining the resolution of the data. As the aircraft flies the magnetometer measure and records the total intensity of the magnetic field at the sensor, which combine the magnetic field generated in the earth and tiny

variations due to the temporal effects of the constantly varying solar wind and magnetic field on the survey aircraft. By removing the solar, regional and aircraft effects, the resulting aeromagnetic map shows the spatial distribution and relative abundance of magnetic minerals in the surface of the earth's crust because distinct rock types differ in their content of magnetic minerals The magnetic map shows the geological structure upper crust in the surface, particularly the spatial geometry of the bodies of rock and the presence of folds and faults. Aeromagnetic use in Geological maps, mineral exploration and also use to perform reconnaissance mapping of unexploded ordnance.

3.7 Units of Magnetic Fields

In the S.I system of units, the magnetic parameters are defined in terms of flow of electric current. A current passing through a coil consisting of several turns of wire produces a magnetic flux that flows through and around the coil annulus. The magnetic flux arises from a magnetizing force $\overrightarrow{H_f}$. The magnitude of $\overrightarrow{H_f}$ is proportional to the number of turns *N* in the coil and the strength of the current *I* and inversely proportional to the length of the wire, *l*. Thus $\overrightarrow{H_f}$ is expressed in units of Ampere per metre (A m^{-1}). The density of the flux (i.e. the number of field lines crossing over an area perpendicular to the direction of flow) is the magnetic induction or magnetic field $\overrightarrow{B}$. This $\overrightarrow{B}$ is actually the same in direction as the total field. The field $\overrightarrow{B}$is proportional to$\overrightarrow{H_f}$, i.e.

$$\vec{B} = \mu\vec{H}$$

Where μ is the permeability of medium. It expresses the ability of the medium to convey a magnetic flux. $\overrightarrow{B}$ Can be expressed in volt second per square metre (Vsm^{-2}) or Weber per square metre (Wbm^{-2}). Where 1 Wbm^{-2} =1tesla (T). Hence the unit of μ becomes $WbA^{-1}m^{-1}$ or Henry per metre (H m^{-1}). The magnetic permeability of vacuum is denoted as μ_0 and has a value of $4\pi \times 10^{-7}$ H m^{-1}. The c. g. s (centimetre-gram-second) unit of

magnetic field strength is the Gauss (G), where 1 G = 10^{-4}T. The equivalent c. g. s of gauss is the gamma (γ), such that 1 γ = 10^{-5}G. The tesla is rather a large unit to express small magnetic anomalies caused by rocks. In this realm, the nanotesla (nT) is employed such that

$1nT = 10^{-9}T$

$1\gamma = 1nT = 10^{-5}G$

The total field magnetic field intensity values for all aeromagnetic maps in Nigeria are expressed in nano tesla or gamma. *B* varies in strength from about 25,000 nT in equatorial regions to about 70,000 nT at the poles (Phillip *et al.,* 2002).

3.8 Reduction to Magnetic Equator

Reduction to the equator is used in low magnetic latitudes to Centre the peaks of magnetic anomalies over their sources. This can make the data easier to interpret while not losing any geophysical meaning. Reducing the data to the pole (REDP) does much the same thing, but at low latitudes, a separate amplitude correction is usually required to prevent North-South signal in the data from dominating the results. As a result, reduced to the pole data may present a less 'honest' view of the data. To reduce magnetic data to equator we apply the equation,

$$L(\theta) = \frac{\left[\sin(I) - i.\cos(I).\cos(D-\theta)\right]^2 X\left(-\cos^2(D-\theta)\right)}{\left[\sin^2(I_a) + \cos^2(I_a).\cos^2(D-\theta)\right] X\left[\sin^2(I) + \cos^2(I).\cos^2(D-\theta)\right]}, if\ (|I_a|) < (|I|), I_a = I \quad (3.1)$$

where

I_a is a magnetic inclination

I_a is an inclination for amplitude correction

D is a magnetic declination

Sin (I) is the amplitude component while icos (I) cos (D-θ) is the phase component

This is a method of removing the dependence of magnetic data on the angle of magnetic inclination. This filter converts data which have been recorded in the inclined earth's magnetic field at the equator to what the data would look like if magnetic field had been vertical.

3.9 Production of Reduction to Pole from TMI

The reduction to pole is used in frequency domain to modify the amplitude correction in the magnetic North- South direction or to estimate an equivalent source in the space domain (Silver *et al.*, 2003).

The reduction to the pole is:

$$L(\theta) = \frac{1}{(\sin I_a + i\cos I.\cos(D-\theta))^2} \qquad (3.2)$$

where

I is a magnetic inclination

I_a Inclination for amplitude correction (never less than I)

D is a magnetic declination

Parameter:

I_a Inclination to use for the amplitude correction. Default is ± 20. (I_a= 20, if I> 0; I_a= (-20), if I< 0). If I_a is specified to be less then I , it is set to I.

It can be observed that as I tend to zero (the magnetic equator) and (D-Θ) tend to $\frac{\pi}{2}$. then the reduce to pole operator tends to infinity (Mendonca and Silver 1993). The problem

addressed by introducing a second inclination (I´) that is used to widget the amplitude of the filter near the equator (Grant Dobbs 1972)

3.10 Horizontal Derivatives

The Horizontal derivative used for the identification of geologic boundaries in the profile data, the horizontal derivative x, y, z direction is denoted dx, dy and dz respectively. The horizontal derivative dx shows the geological structure in y direction, horizontal derivative of dy shows the geological structure in x direction and horizontal derivative dz shows the geologic structure both in x and y direction.it is mathematically express as

$$L\,(V) = (Vi)^n \tag{3.3}$$

where n is the order of differentiation and i= $\sqrt{-1}$

3.11 Vertical Derivative

The vertical derivative is usually applied to total magnetic field data to increase the shallow geologic source in the data like other filter increasing the high wave number component of the spectrum, also in the application of low-pass filter to remove high wave number noise.

$$L\,(r) = r^n \tag{3.4}$$

Where n is the order of differentiation. And r is the wave number (radians/ground unit) Note: r = 2pk where k is cycles/ground unit. Ground unit is the survey ground units used in your grid (e.g. meter, feet etc.). The vertical derivative is commonly applied to total magnetic field data to enhance the shallowest geologic sources in the data. As with other filters that enhance the high-wave number components of the spectrum, you must often also apply low-pass filters to remove high-wave number noise.

3.12 Tilt Derivative

Tilt derivative is used to obtain a good estimation of both the location and depth of magnetic sources. The tilt derivative and horizontal derivative are total horizontal derivative are utilized for mapping shallow basement structure and mineral exploration targets. The tilt derivative is mathematically defined as

TDR=$\tan^{-1}[\frac{VDR}{THDR}]$ Where VDR is the first vertical derivative

THDR is the total horizontal derivative of total magnetic intensity VDR= $[\frac{dT}{dz}]$

And total horizontal derivative is THDR= $\sqrt{\left(\frac{dT}{dx}\right)^2 + \left(\frac{dT}{dy}\right)^2}$ (3.5)

3.13 Analytical Signal

The filter applied to magnetic data for the purpose simplifying the magnetic bodies normally have positive and negative peak joined with its, which is not make it easy to determine the exact location of causative body. The bell-shaped symmetrical function is derived for two dimensional bodies and which amplified of analytical signal is for three dimensional bodies. This function and it derivative are not depend on strike dip magnetic declination, inclination, and remnant magnetization (Debeglia and Corpel, 1997) the 3-D analytic signal at location (x,y) can be obtained from three orthogonal gradients of total magnetic field using these expression

$|A(x,y)| = \sqrt{\left(\frac{dT}{dx}\right)^2 + \left(\frac{dT}{dx}\right)^2 + \left(\frac{dT}{dx}\right)^2}$ (3.6)

where $|A(x,y)|$ is the amplitude of the analytic signal at (x,y)

T is the observe magnetic field at (x,y)

dx is the horizontal derivative over a 2-D magnetic contact located at (x=0) and at depth h is described by the expression shown below

$$|A(x)| = \alpha \frac{1}{[h^2+x^2]^{1/2}} \quad (3.7)$$

where α is the amplitude factor

$\alpha=2M\sin d\,(I-\cos^2(I)\sin 2(A)$

h is the depth to the top of the contact

M is the strength of magnetization

d is the dip of the contact

I is the inclination of the magnetization vector

A is the direction of the magnetization vector

The above equation described the analytic signal for simple bell-shaped function.

Note that: the amplitude of the peaks is directly proportional to the magnetization at the edge as defined by the equation above.

The horizontal derivative is calculated by applying a space domain convolution filter, the Fourier transform of a space domain-function f(x) is mathematically define as

$$f(w)=\int_{-\infty}^{\infty} f(x)\, e^{iwx} dx \quad (3.8)$$

And in frequency domain is define as

$$f(x)=\frac{1}{2\pi} f(w) e^{-iwx} dx \quad (3.9)$$

where w is an angular wave number in radian per unit ground unit (Ma Clellan and Nawab, 1979) it is possible to present this data in two dimensional (2-D) Fourier series.

The Fourier series contains terms of different frequencies that joined together to form the potential field data. The amplitude and phase relation are called complies line spectrum (Bhattachaya, 1966) this relationship governs the Fourier series and it is normally use for the interpretation of magnetic data. A periodic function f(x) of the independent variable the dimension of it length may be expressed in a Fourier series as shown below.

$$f(x) = \frac{a_0}{2} + \sum_{n=1}^{\infty} \left(a_n \cos \frac{n\pi x}{L} + b_n \sin \frac{n\pi x}{L} \right) \quad (3.10)$$

Where w is the fundamental angular frequency given by w=2π/x and x is the total length of x over which f(x) has been measured, the coefficient a_0, a_n, and b_n are define as follows

$$a_0 = 1/x \int_{-x/2}^{x/2} f(x) dx \quad (3.11)$$

$$a_n = 1/x \int_{-x/2}^{x/2} f(x) dx \quad (3.12)$$

$$b_n = 1/x \int_{-x/2}^{x/2} f(x) dx \quad (3.13)$$

The above equation can also be writing in exponential form such as

For discrete time Fourier transform (DTFT)

$$F(x) = \sum_{n=\infty}^{2} f(n) e^{inwx} \quad (3.14)$$

For continuous time Fourier transform (CTFT)

$$F(x) = \frac{1}{x} \int_{-x/2}^{x/2} f(x)\, e^{inwx} dx \quad (3.15)$$

3.14 The Centre for Exploration Targeting (CET) Grid Analysis Plug-In for Structures

Stating with standard deviation that provide an estimate of the local variation in the data. At each location in the grid, it calculates the standard deviation of the data values within the local neighborhood. Features of significance often exhibit high variability with respect to the background signal. For a window containing N cells, whose mean value is μ, the standard deviation σ of the cell values x_i is given by:

$$\sigma = \sqrt{\frac{1}{N}\sum_{i=1}^{N}\left(x_{i-\mu}\right)^2} \tag{3.16}$$

When interpreting the output, values which approach zero indicate very little variation, whereas large values indicate high variation. Kovesi (1996). The next stage is to apply **Phase Symmetry;** this property is useful in detecting line-like features through identifying axes of symmetry. It is also known that the symmetry of a signal is closely related to the periodicity of its spatial frequency. Consequently, it is natural to utilize a frequency-based approach to detect axes of symmetry. This plug-in implements the phase symmetry algorithm developed by Kovesi (1996).

In the one-dimensional case (1D), a point of symmetry in the spatial domain corresponds with a point where local frequency components are at either a minimum or a maximum. To identify points of symmetry in two-dimensional (2D) data we first break the data into 1D profile and analyze these over multiple orientations at varying scales. For example, a line-like feature will produce strong symmetry responses from the 1D profiles sampled from all orientations except for those parallel to the line. The result from phase symmetry is passed through Amplitude Thresholding**,** in conjunction with non-maximal suppression (NMS). The NMS is useful for finding ridges since low values are suppressed whilst

points of local maxima are preserved, it also considers the local feature orientation so that the continuity of features is maximized and can be used to remove noise and highlight linear features. A description of the NMS algorithm is given below.

For each cell in the grid, it examines the values at a distance, *r*, in the directions perpendicular to the local feature orientation - the local feature orientation is typically the direction in which a ridge or valley is running. If the cell has a value greater than those on either side of it, the cell is kept since it is a local maximum; otherwise it is set to zero.

The Amplitude Threshold plug-in applies the above algorithm followed by a threshold step. Threshold marks cells in grid as either 'foreground' or 'background' cells depending on whether the cell value is greater or less than a specified threshold value respectively. Thus, threshold will reduce a grid to a binary grid of only two distinct cells values: 1 for regions of interest and a dummy value for background. In this suite of tools, Amplitude Threshold is useful for reducing phase symmetry or phase congruency output to a grid depicting only trend lines.

Finally, Skeleton to Vectors is applied. The Skeleton to Vectors plug-in is for vectorising the skeletonised structures from the skeletonisation plug-in via a line fitting method described below. This vectorised data can then be used as input to the structural complexity map plug-ins. For each structure in the grid, a line is formed between its start and end points. If the structure deviates from this line by more than a specified tolerance the structure is divided into two at the point of maximum deviation and the line fitting process is repeated on these two new structure segments. This process is continued recursively until no structure segment deviates from its corresponding line segment by more than the specified tolerance. These line segments form the vectorised representation of the structures within the grid. Lam *et al (*1992).

3.15 Susceptibilities of Rocks

The content of magnetite in rocks determine it susceptibility, sediments and igneous rocks have weak magnetite which lead to small susceptibilities whereas Basalts, Gabbro's and Serpentinities are possess strong magnetic. Weathering are usually affecting the susceptibility of material because magnetite is oxidized to hematite but some laterites are magnetic because its posse of maghemite and remnant magnetized hematite, the table below show the magnetic susceptibilities of common rocks (John Milson).

Table 3.1: Magnetic Susceptibilities of Common Rock

Common rocks	Magnetic susceptibilities
Slate	0-0.002
Dolerite	0.01-0.15
Basalt	0.001-0.1
Limestone	0.00001-0.0001
Greenstone	0.0005-0.001
Granulite	0.0001-0.05
Rhyolite	0.00025-0.01
Salt	0.0-0.001
Gabbro	0.001-0.1

3.16 Theory of Radiometric Survey

Radiometric surveys detect and map natural radioactive emanations, called gamma rays, from rocks and soils. All detectable gamma radiation from earth materials come from the natural decay products of only three elements, i.e. uranium (U), thorium (Th), and potassium (K). In parallel with the magnetic method, that is capable of detecting and mapping only magnetite (and occasionally pyrrhotite) in soils and rocks, the radiometric method is capable of detecting the presence of U, Th, and K at the surface of the ground.

The basic purpose of radiometric surveys is to determine either the absolute or relative amounts of U, Th, and K in the surface rocks and soils. No other geophysical method, and probably no other remote sensing method, requires consideration of so many variables in order to reduce the observational data to a form that is useful for geological interpretation. Meteorological conditions, the topography of the survey area, the influence of the planets cosmic environment, the height of the sensor above ground and the speed of the aircraft are just a few of the variables which affect radiometric measurements, and which can bias an analysis unless dealt with very thoroughly. A few of the benefits that could be expected from the interpretation of radiometric surveys include:

i. Changes in the concentration of the three radio elements U, Th, and K accompany most major changes in lithology; hence the method can be used as a reconnaissance geologic mapping tool in many areas.
ii. Variations in radioelement concentrations may indicate primary geological processes such as the action of mineralizing solutions or metamorphic processes.
iii. Variations also characterize secondary geological processes like supergene alteration and leaching.
iv. Radiometric surveys are capable of directly detecting the presence of uranium.
v. This data can also assist in locating some intrusive related mineral deposits.

In appropriate areas, when used as a reconnaissance technique for mapping geology and for prospecting, the cost/benefit ratio for airborne radiometric surveying is nearly as good as that for airborne magnetometer surveying. (Geosiam).

3.17 Some Factor Affecting Concentration of Radioelement (K, U and Th)

i. Weathering
ii. Alteration

iii. Climate Condition

iv. Hydrothermal Process (IAEA, 2003)

Like hydrothermal processes can result in variations of the radioelement content of the host rocks and among the three radioelements, Potassium K is mostly affected by such process while Thorium Th is less often and Uranium U very infrequently. Potassium is usually increased during alteration signature but weathering generally decreases the intensity of alteration signature. (Dickson and Scott, 1997). Thorium Th usually consider as a stable which does not move easily. However, several deposits of gold depict increases in Potassium and Thorium which suggested that thorium was move during hydrothermal activities (Silva *et al* .2003). Reduction in thorium and increase in potassium K indicate a sign of alteration for most deposits of ore (Ostrovskiy, 1975) and it for this reason the Thorium map and Uranium image ratio (U/K) map was developed to show good definition in mapping the granitoid rocks show low uranium but high potassium concentration.

CHAPTER FOUR

4.0 RESULTS AND DISCUSSION

4.1 Total Magnetic Intensity (TMI) Map Production

The gridded aeromagnetic data obtained from NGSA whose parameter where stated above were gridded using minimum curvature mode on the Oasis Montaj and display in color aggregate map (Figure 4.1). The map exhibits the various magnetic susceptibility that constitute the lithology within the area. Being an area that is close to the equator the effect of earth's field plays a significant role in variation of susceptibility; areas with high magnetic susceptibility are showing high magnetic values while regions with low magnetic value depict low magnetic susceptibility. Magnetic values within the area range from -119 nT to 147.9 nT. The lower end of the southern region shows relatively low susceptibility this cannot be remove from the level of sedimentation within the terminal end of Bida clusters of highs and lows dominate the field though no much pronounced within the Bida sheet (163). The eastern end depicts a lot of pronounced activity due to the close variations in field susceptibility.

4.2 Total Magnetic Intensity (TMI) - Reduction to the Equator (RTE)

The computed TMI-RTE helps in producing the symmetry for anomaly that exhibits dipolar nature due to non-vertical inducing field. Equally it places the anomalies from the residual field directly above the causative bodies/rocks. (Figure 4.2) depicts both positive and negative anomalies coming from magnetic rocks within the region.

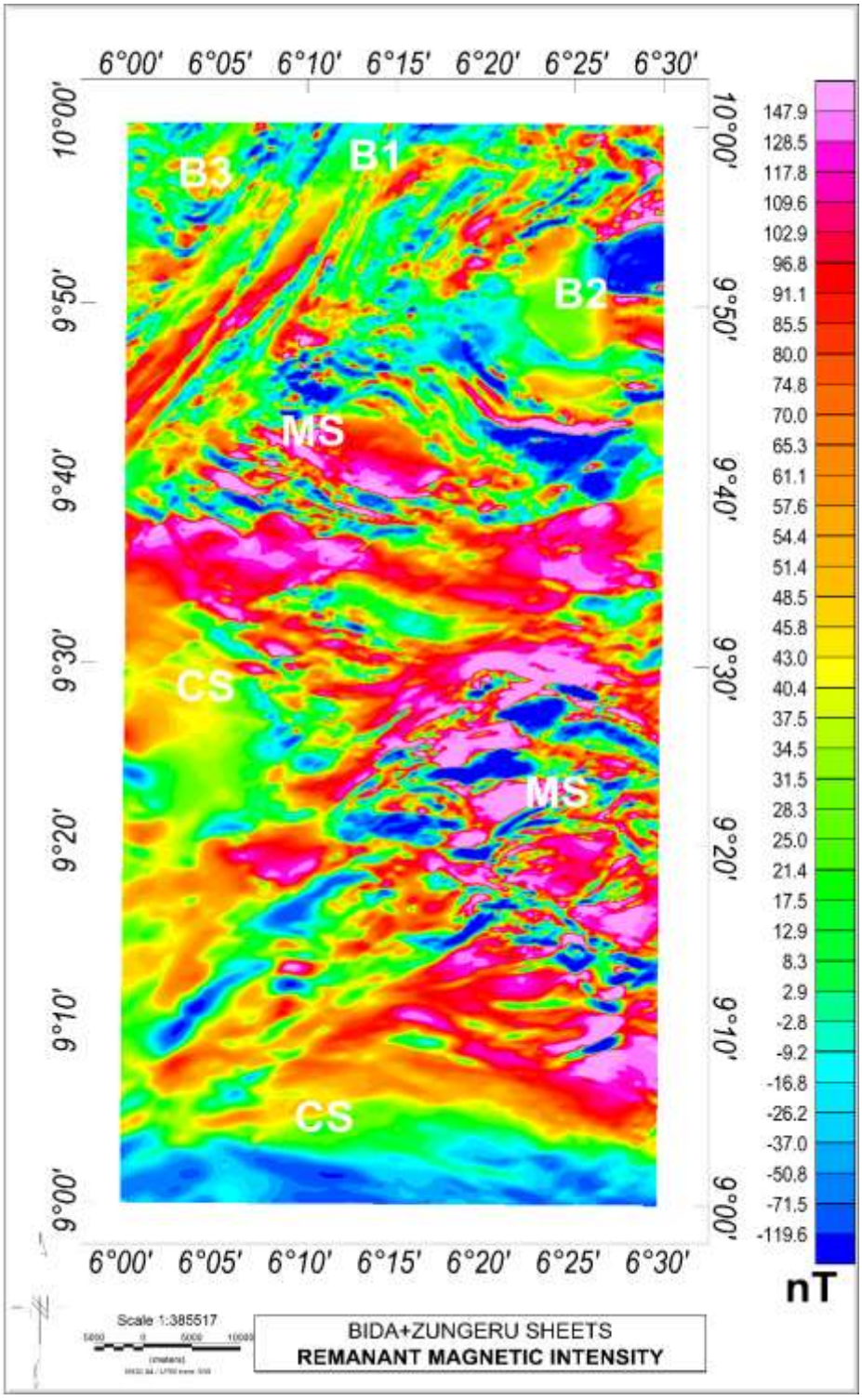

Figure 4.1: Total magnetic intensity map of the study area (Bida and Zungeru) with IGRF of 33000 nT removed.

The cretaceous sediment at the lower part of the study area shows low susceptibility due to overlaying sedimentation. The meta-sediments at the mid-eastern part of the area shows appreciable high susceptibility this is general due to intrusive activities of undifferentiated

granite. The belt type schist and mylonites also shows some appreciable susceptibility (Figure 2.2).

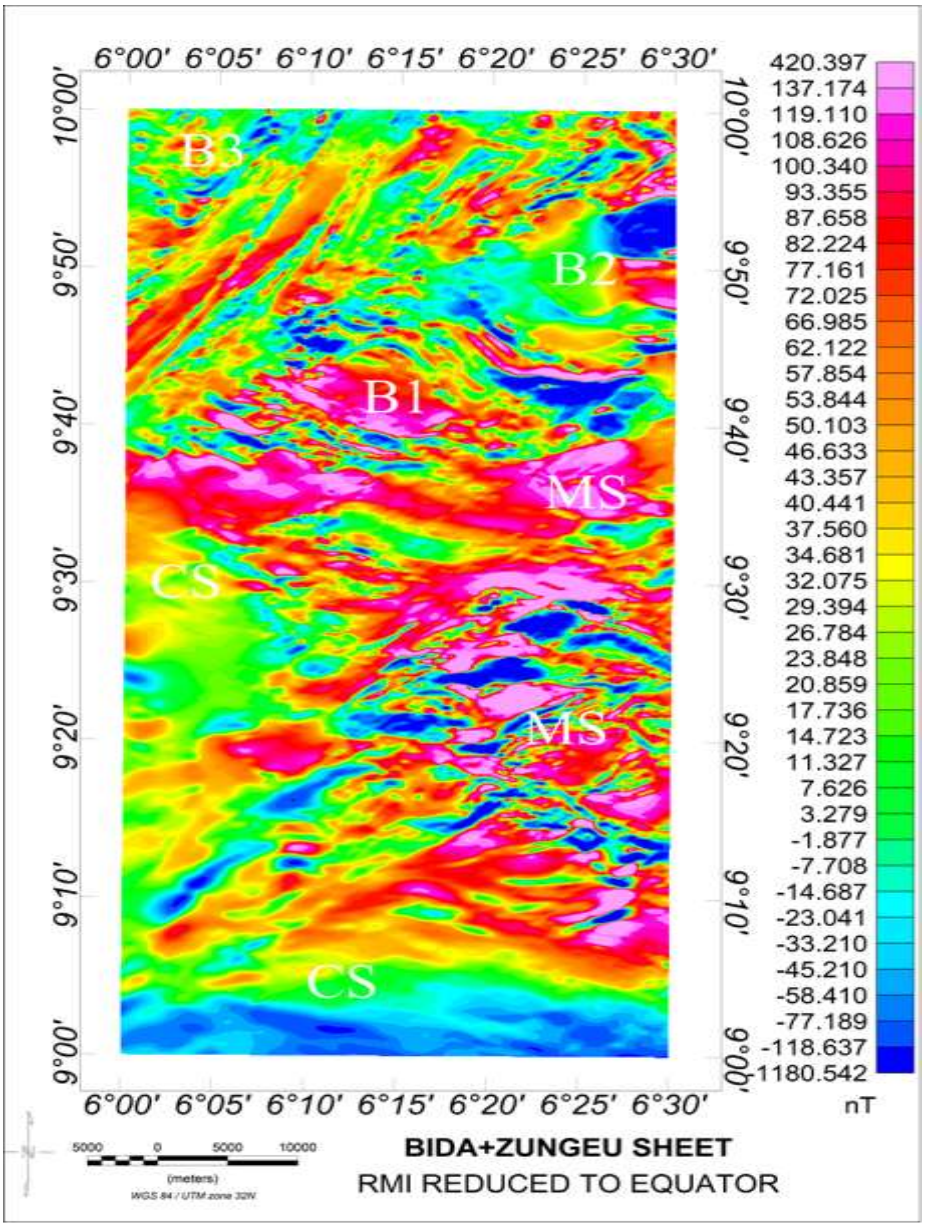

Figure 4.2: Total magnetic intensity (TMI) - reduce to equator (RTE) map of Bida and Zungeru

4.3 Horizontal Derivatives (Dx, Dy and Dz)

The horizontal derivation maps (Figure 4.3a, 4.3b and 4.3c) were reveal a clear demarcation between the region of cretaceous sediment and metasediment base on degree of distortion to the magnetic signature. An evenly well oriented magnetic signature within

the sedimentary formation at the lower up to the western end of the study area while the metasediment regions are noted for a high distortion to the magnetic signature approximately in y direction. This depicts a mixture of highs and low susceptibility of short-wave anomalies in a high frequency of occurrence around upper edge of the SE signifying highly weathered of biotite granite when correlate with geology map of the study area Figure 2.2, NW and NE edge of the study area. The outcrop of B1 and B2 clearly marked out on the geology map as an intrusion of biotite granite and major discontinuities exist below B1. While horizontal derivative map (Dy) shows the one lies in x-direction and Dz shows magnetic signature in both x and y direction.

4.4 Analytical Signal

The analytical signal map was carefully computed to attenuate sources showing negative susceptibility for clearer interpretation. The 3D analytical signal requires the horizontal derivatives in x, y and z but the z component was achieved in frequency domain after Fourier transform. Analytical signal helps remove the dependence of the residual field on the angles of declination and inclination, thereby positioning the anomaly at the center of the causative body. The resulting Figure 4.4 shows the regions of meta-sediments having high amplitude signal, a clear indication that the amplitude signal is a reflection of magnetisation of the causative body

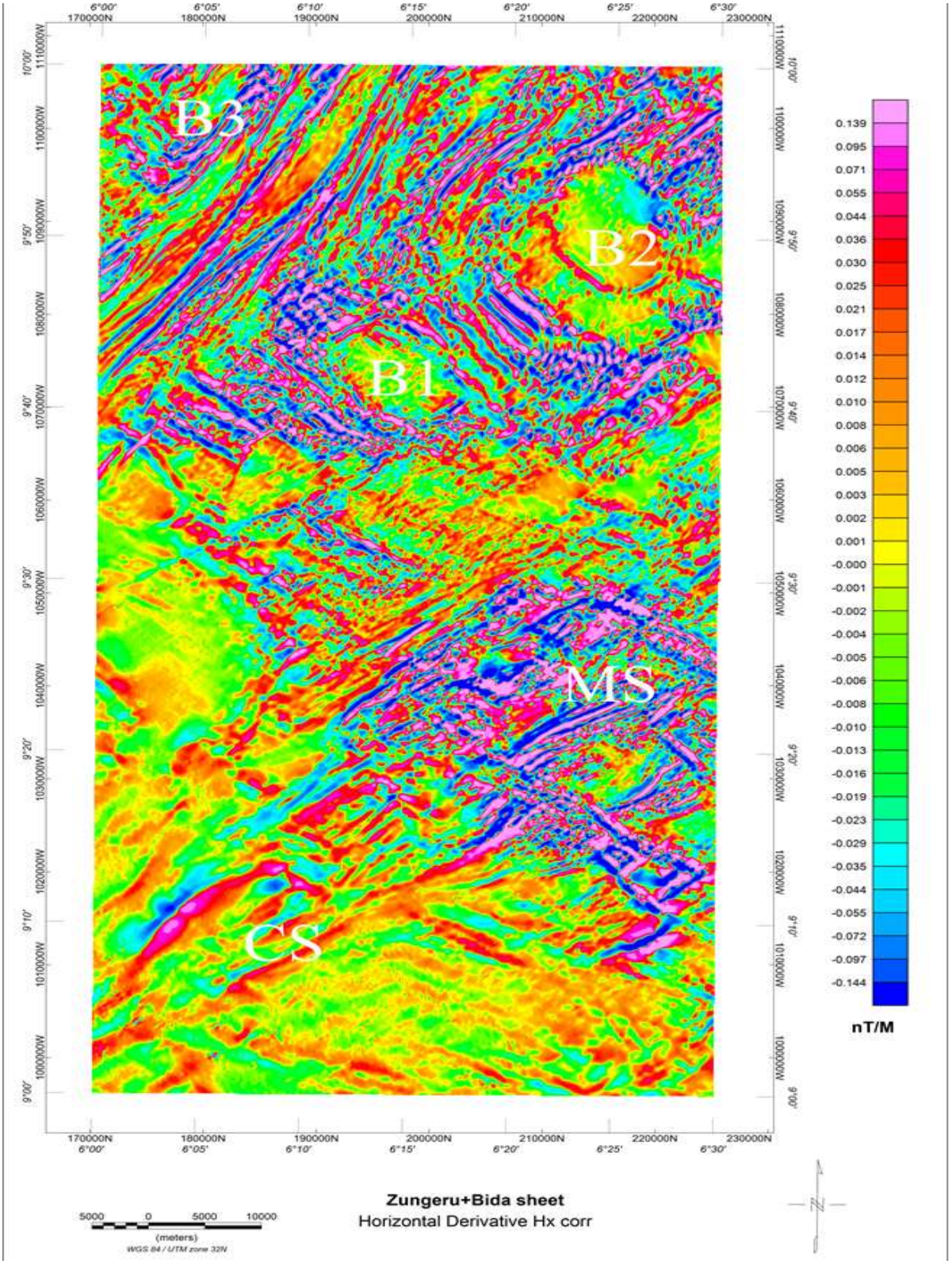

Figure 4.3a Horizontal derivative map (Dx) of Bida and Zungeru

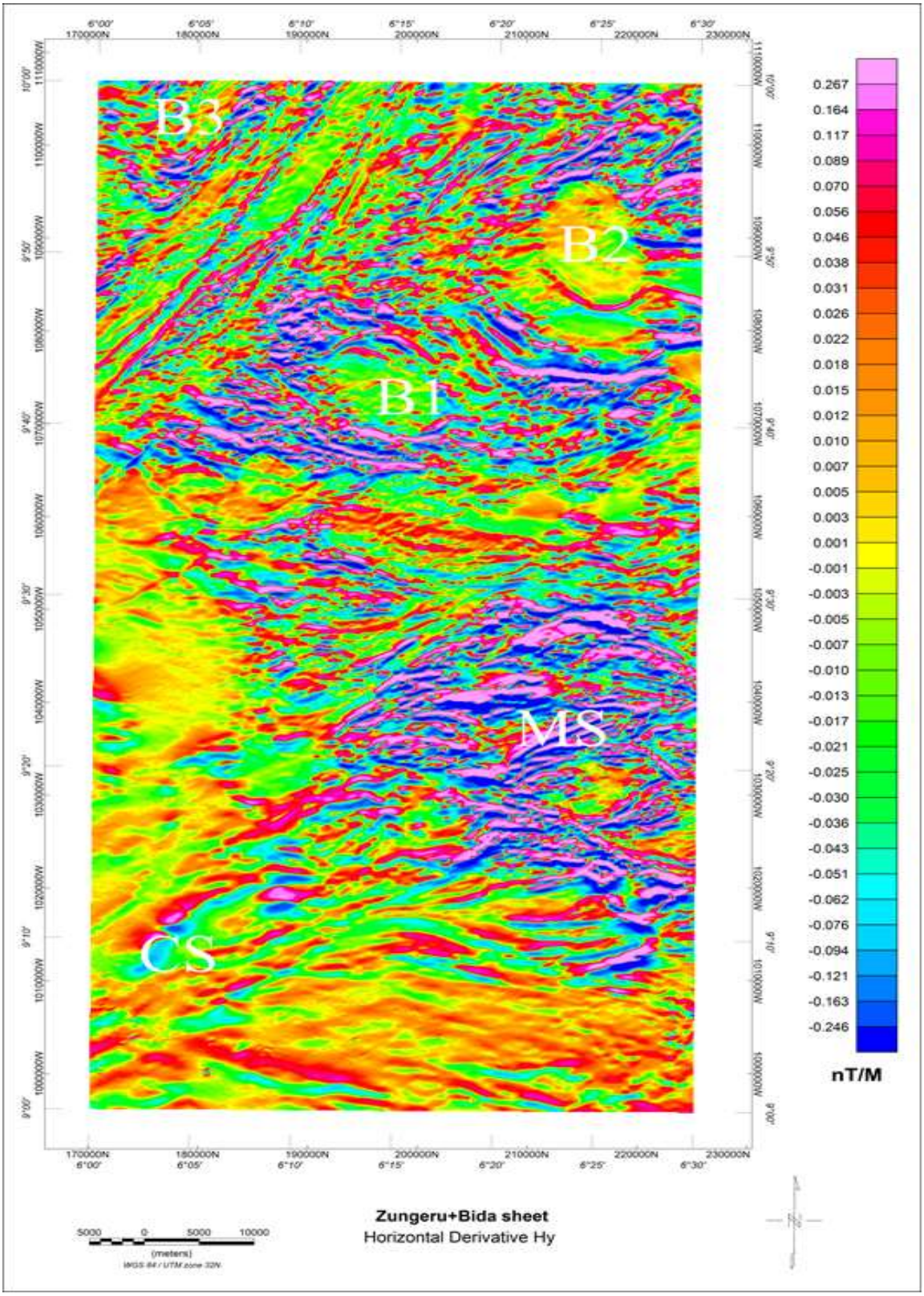

Figure 4.3b Horizontal derivative map (Dy) of Bida and Zungeru

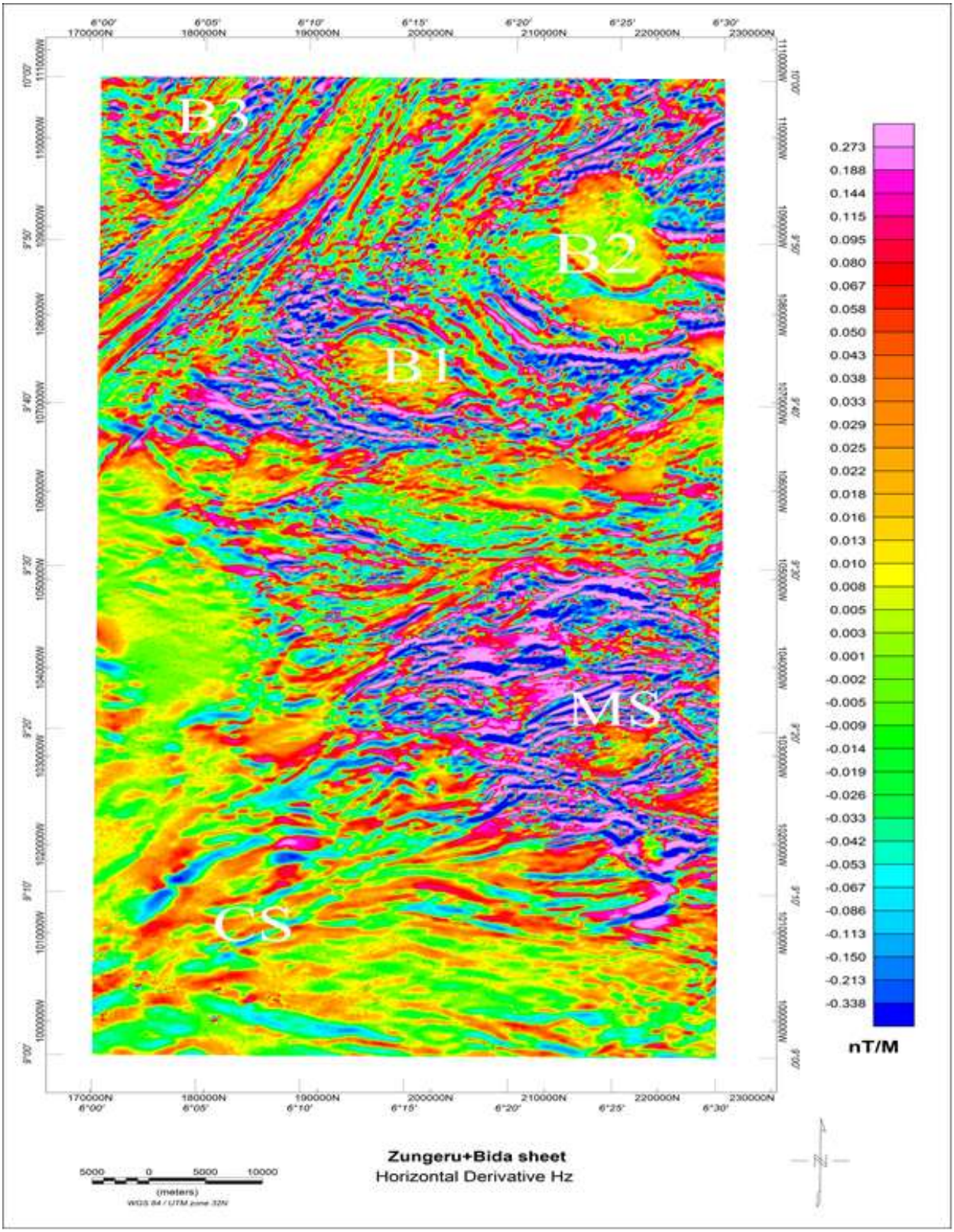

Figure 4.3c: Horizontal derivative map (Dz) of Bida and Zungeru

(Nabighian 1972, Roset and Pikington 1992). A clear demarcation is observed between the cretaceous sediment at the lower part and regions of meta-sediments that has undergone several degree of deformation. The weak magnetic susceptibility values within the meta-sediments depicts felsic intrusive formations such as B2 and MS, while strong magnetic susceptibility within same meta-sediments are regions of malfic intrusive bodies such as MS, B1 and B3. Significant linear structures at the western corner of the area, and these lineaments are at the contact between different geological formations.

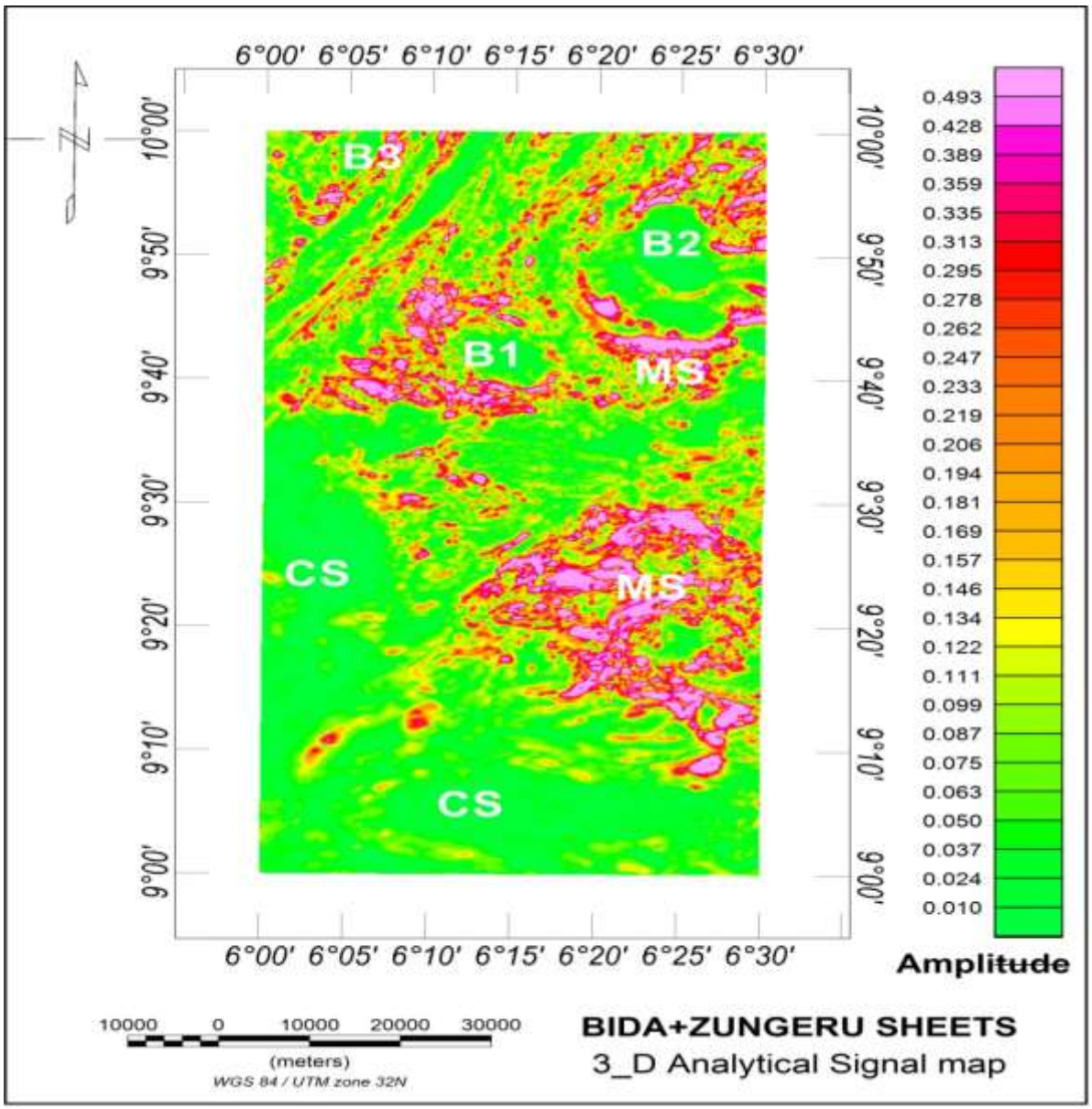

Figure 4.4: Analytical signal map of Bida and Zungeru

4.5 First Vertical Derivative (1VD)

The first vertical derivative map Figure 4.5 is quite revealing a clear demarcation seen between the region of cretaceous sediment and the metasediments base on degree of distortion to the magnetic signatures. An evenly well oriented magnetic signature exists within the sedimentary formation at the lower up to the western end of study area, while the meta-sediment region is noted for a high distortion to the magnetic signatures, which depicts a mixture of highs and low susceptibility of short-wave anomalies in a high frequency of occurrence. The outcrop B1 and B2 clearly marked out on the geology map as an intrusion of biotite granite. Major discontinuities exist below B1 through more clearly demarcated on the grey scale of 1VD.

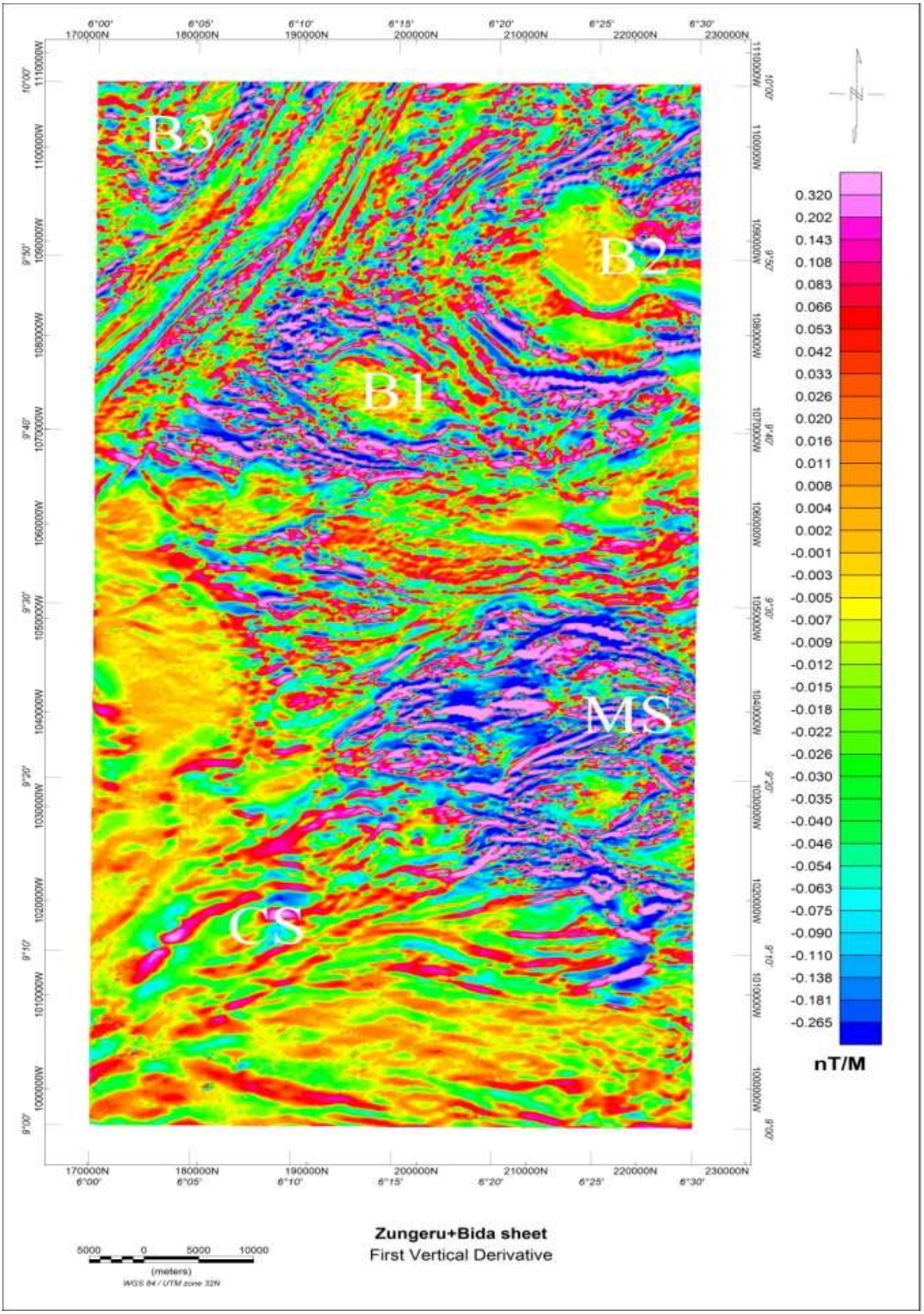

Figure 4.5a: First vertical derivative of Bida and Zungeru

4.6 First Vertical Derivative (Greyscale)

The first vertical derivative models help in retaining long wavelength of the magnetic anomaly field and this is important in improving closely spaced resolution and superimposed anomalies (Pierre, 1995). Contrary, in area with strong distortion in geology and highly weathered outcropping, magnetic sources such as in the area where this research is carried out, direct vertical derivative could come up with noisy results for this reason an appropriate upward continuation of 100 meters was applied to the TMI-RTE before carrying out the 1VD. The result of the 1VD in Figure 4.5b display are vivid picture of observed structural features such as lineaments F1-F6 both on high region of susceptibility (in red) and low regions of susceptibility (in blue) geology contacts (yellow), folds (bold yellow) all across the field prominently at the North-Western corner of the study area are sets of linear structure that trend NE-SW, located within the mylonites and mylonites interlayer by amphibolites which are the belt-type meta-sediments. Equally worth mentioning are set of lineaments (in blue) trend E-W all across the mid region of the study area, where majority of volcanic activities must have been recorded.

The prominent features clearly unavoidable are the spherically shaped intrusive bodies at the upper part of the study area marked by B1 and B2. Interestingly these intrusive bodies show relatively low susceptibility. All the folds delineated are located and the edge/contact between the cretaceous sedimentary formation and the meta-sediment basement region.

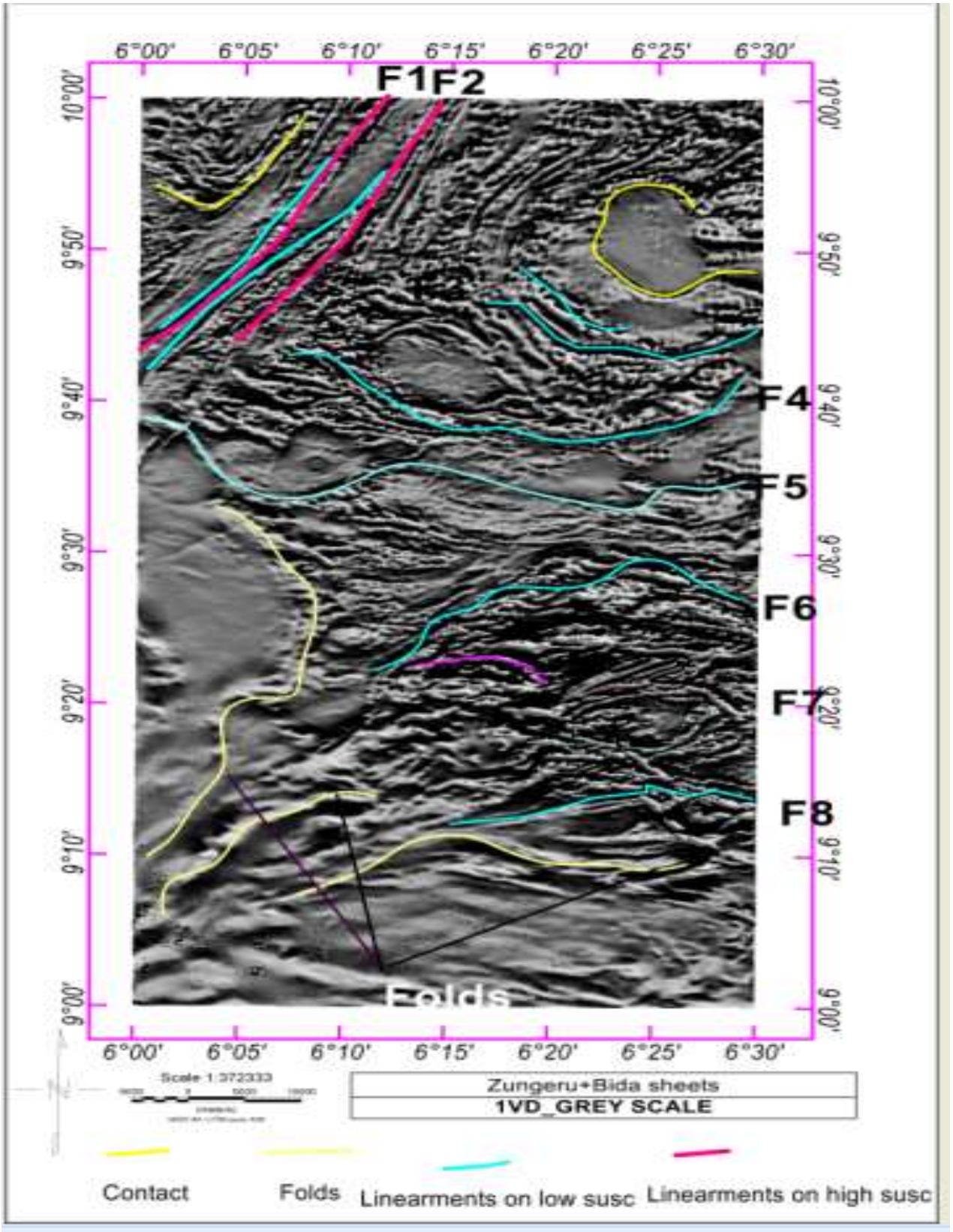

Figure 4.5b: First vertical derivative (Greyscale) of Bida and Zungeru

4.7 Euler Deconvolution

Euler Deconvolution is a depth estimation method that takes advantage of the structural index relating to either a vertical pipe, dyke contact within a complex geological formation index value such as 0, 1 and 2 are assign for bodies like contact, Dyke and pipe respectively. In this analysis structural index of 0, 1, 2 were combined and the result filter so as to accommodate the objectives delineating structures that are host to gold and other associative minerals such as silver.

Results from (Figure 4.6) the analysis shows that majority of these structures are situated between 30 to 300meters all across the field within the metasediment. Generally, depth estimate within 30 to 160 meters dominate the field most especially around Sabon-Dagga, Kakaki, Bobo Shiri, Sunbwagi, Mikwegi and Minkwoigi

4.8 Centre for Exploration Targeting (CET)

Centre exploration targeting is an automation method of delineating lineaments. The results from CET (Figure 4.7) interestingly correlate the lineaments mapped on the 1VD though more detail than that what was observed on the first vertical derivative, Figure 4.5. An added advantage is that the Centre exploration targeting was able to extract the coordinates where these lineaments were observed. Coordinate of these major structures and lineaments that shows degree of mineralisation have been mapped on Figure 4.6 most interestingly is between longitude 6˚20E to 6˚30E and latitude 9˚10N to 9˚30N.

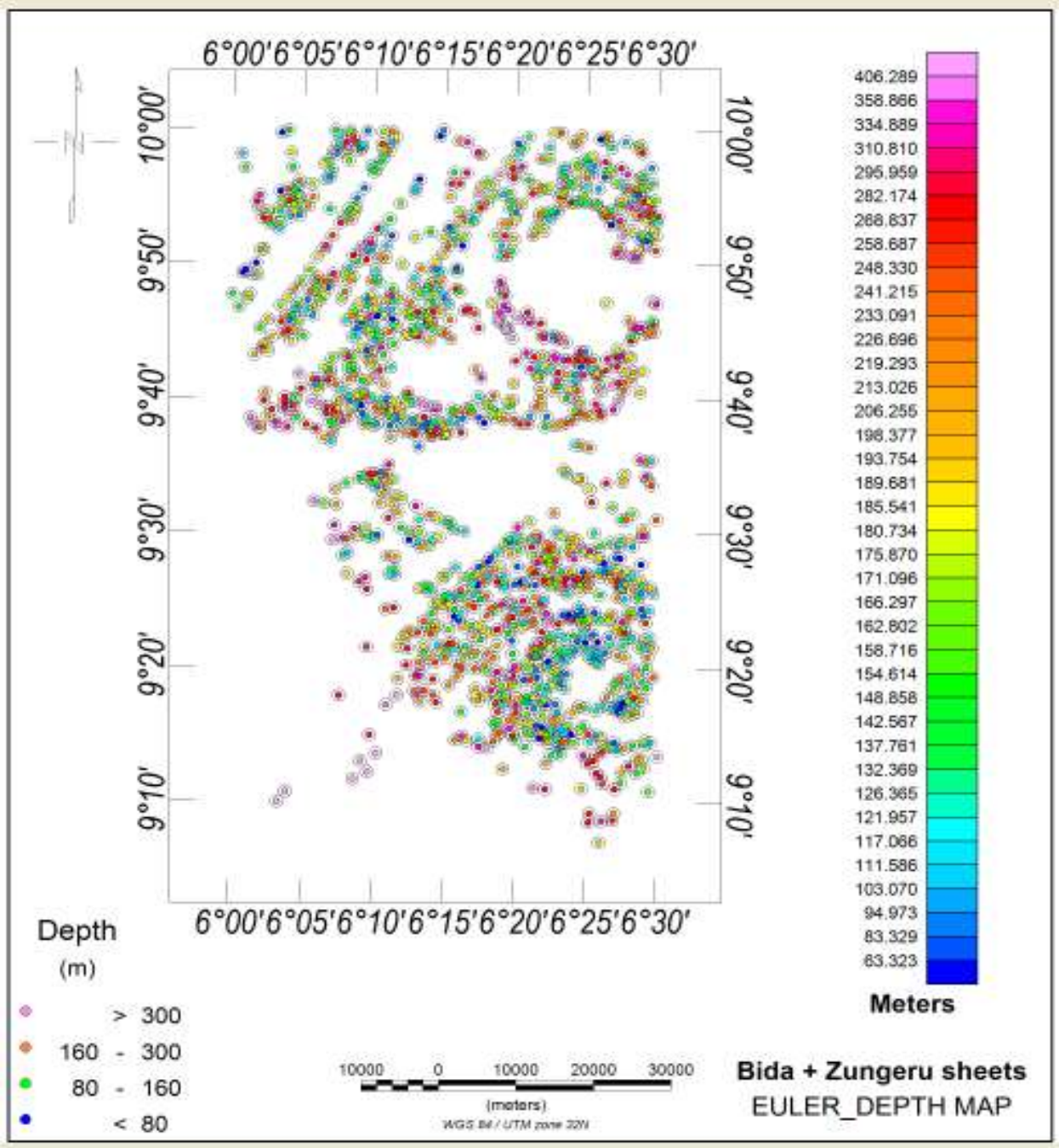

Figure 4.6: Euler depth map of Bida and Zungeru

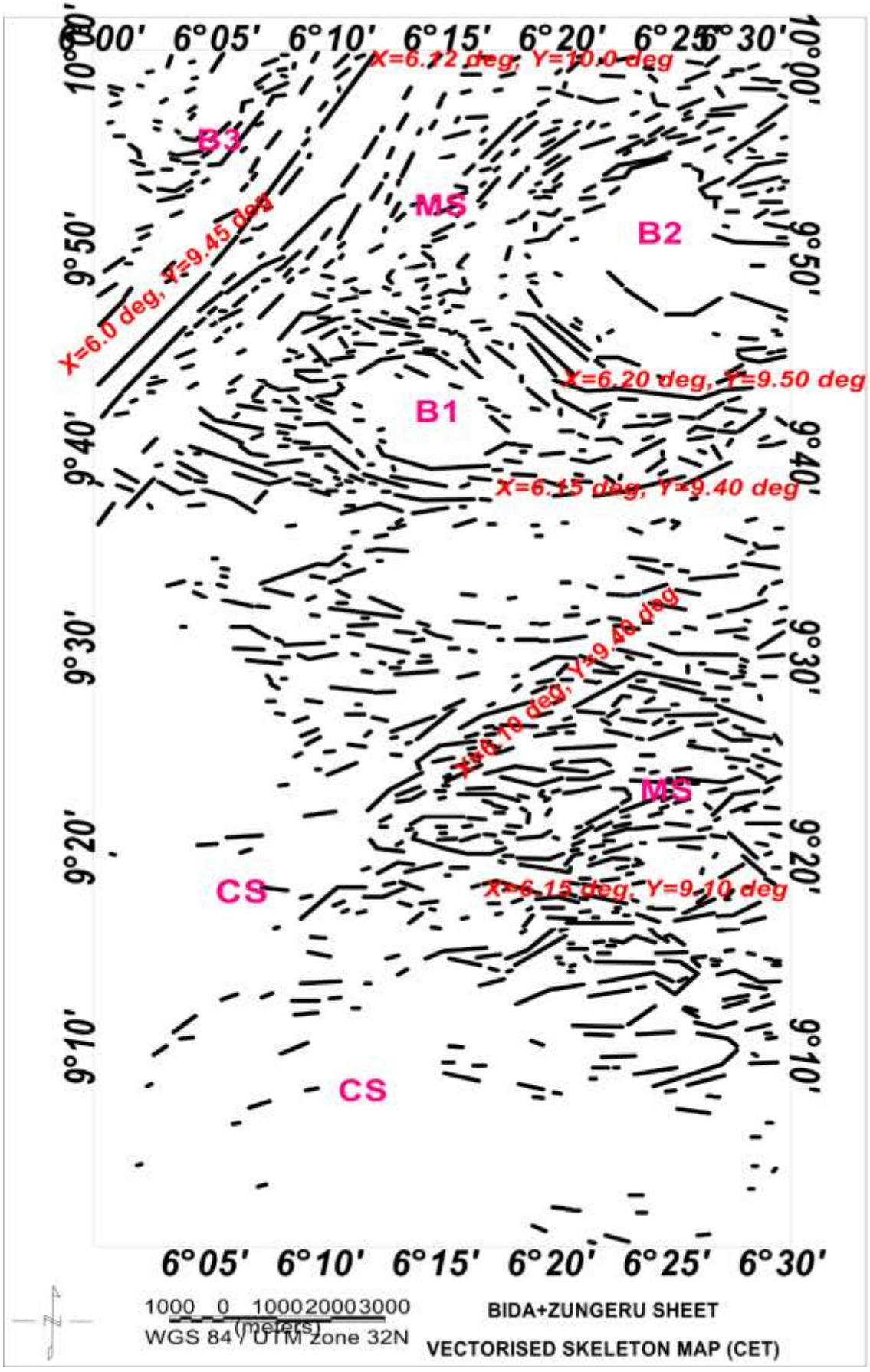

Figure 4.7: Centre exploration targeting map (CET) of Bida and Zungeru

4.9 Interpretation of Radiometric Data

Variations in the mineral constitute of the surface lithology is better reflected in the radiometric survey data, which can be employed in delineating lateral variation in geology. Radiometric survey targets concentration of gamma radiation emanating from mineral forming rocks, these gamma radiations considered are thorium, potassium and uranium.

4.10 Potassium (K) Thorium (Th) and Uranium (U)

Three gamma decay data were considered for analysis, they are potassium, thorium and uranium (Figures 4.8, 4.9 and 4.10). Radiation for potassium originates from potassium feldspar predominantly mica including mylonite muscovite and biotite (Boadi *et al.*, 2013), which are widespread within the felsic breccia of metasediments (MS). These regions depict high anomaly signals at the upper north and eastern part of the study area, worthy of note is another high anomaly notice within the Alluvium deposits at the lower Bida sheet. This coincides with the channel of tribute river-wuya, where erosion has exposed the metasediment basement rocks. Low anomaly signatures where observed within the cretaceous sediments has fairly low potassium K concentration around the western end and southern part of the study area. The thorium concentration map (Figure 4.9) illustrates clearly lithology distinctions. A clear demarcation between the cretaceous sediment shows fairly high anomaly represent the mylonite, amphibolites and granite at the upper north western corner of the study area. Show a high anomaly of thorium concentration. Bodies define as B1, B2, B3 are on high concentration. Low anomalies of thorium are evident at the middle of the study area within the metavolcanics and pebbly schist.

The uranium concentration gives a fairly similar picture to that of the thorium, from the southern end to the western end up to the north western corner depicts fairly high anomaly. While the eastern end shows low anomaly with some isolated highs on intrusive bodies name as B1, B2.

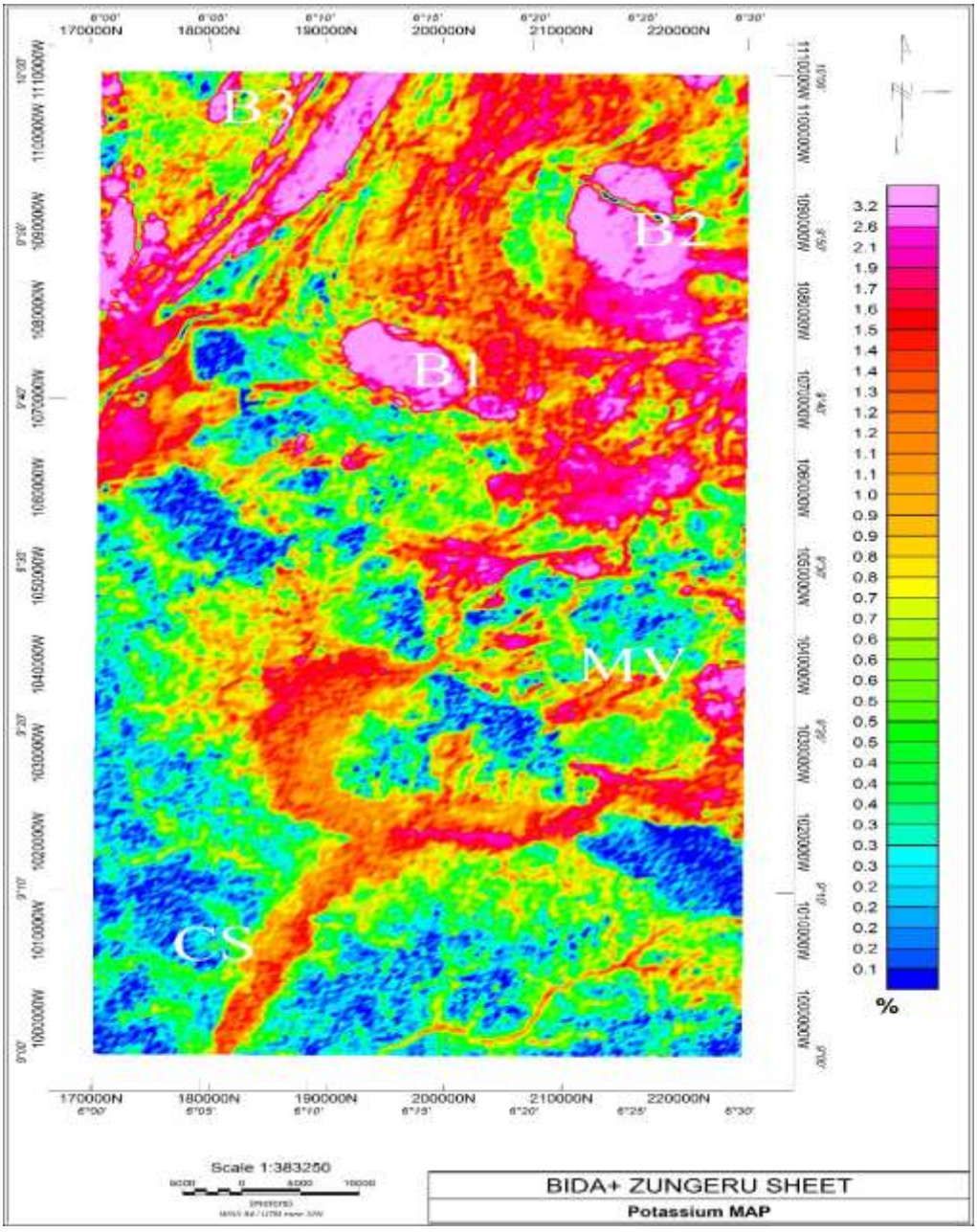

Figure 4.8: Potassium concentration map of the radiometric data of Bida and Zungeru

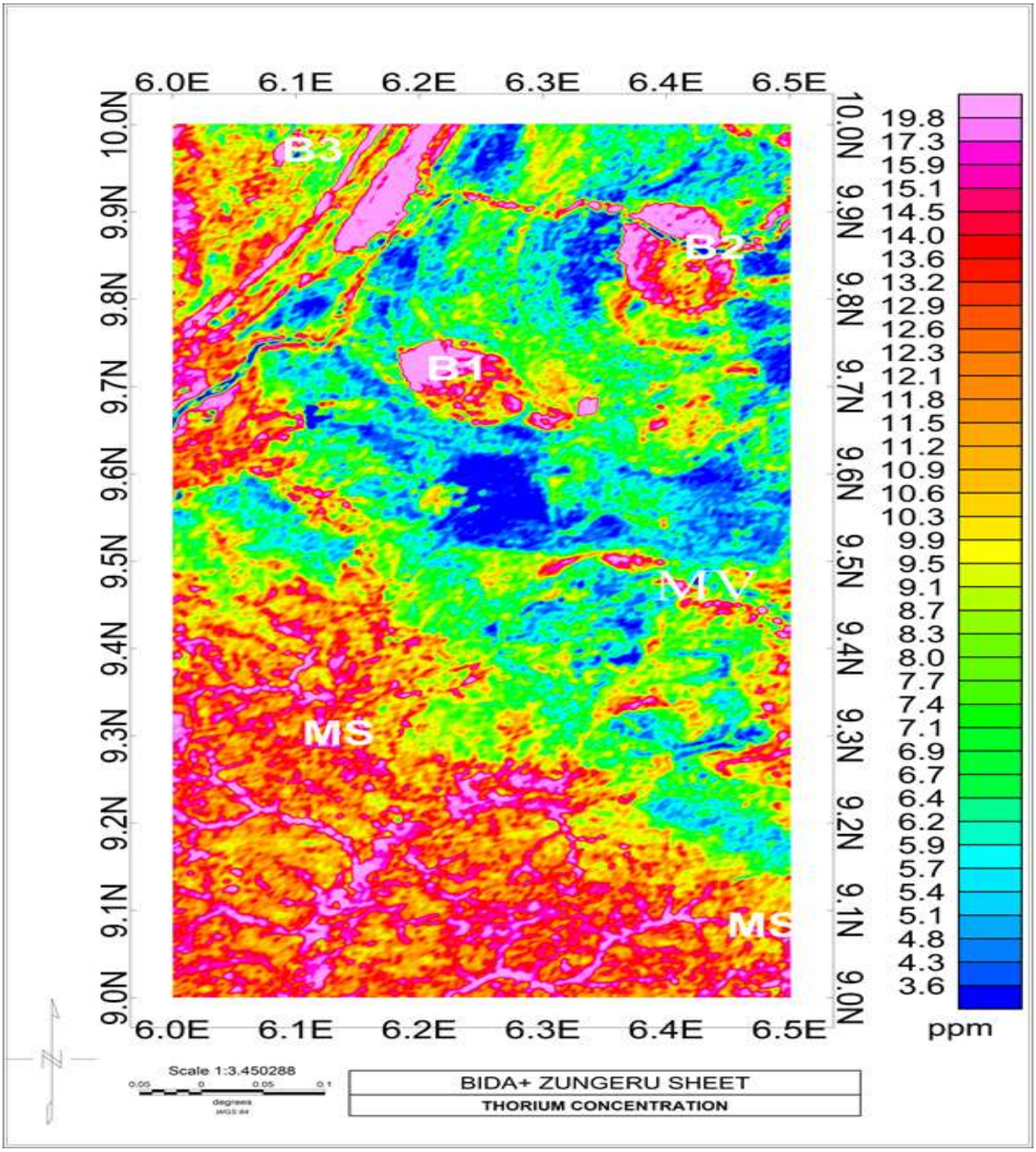

Figure 4.9: Thorium concentration map of the radiometric data of Bida and Zungeru

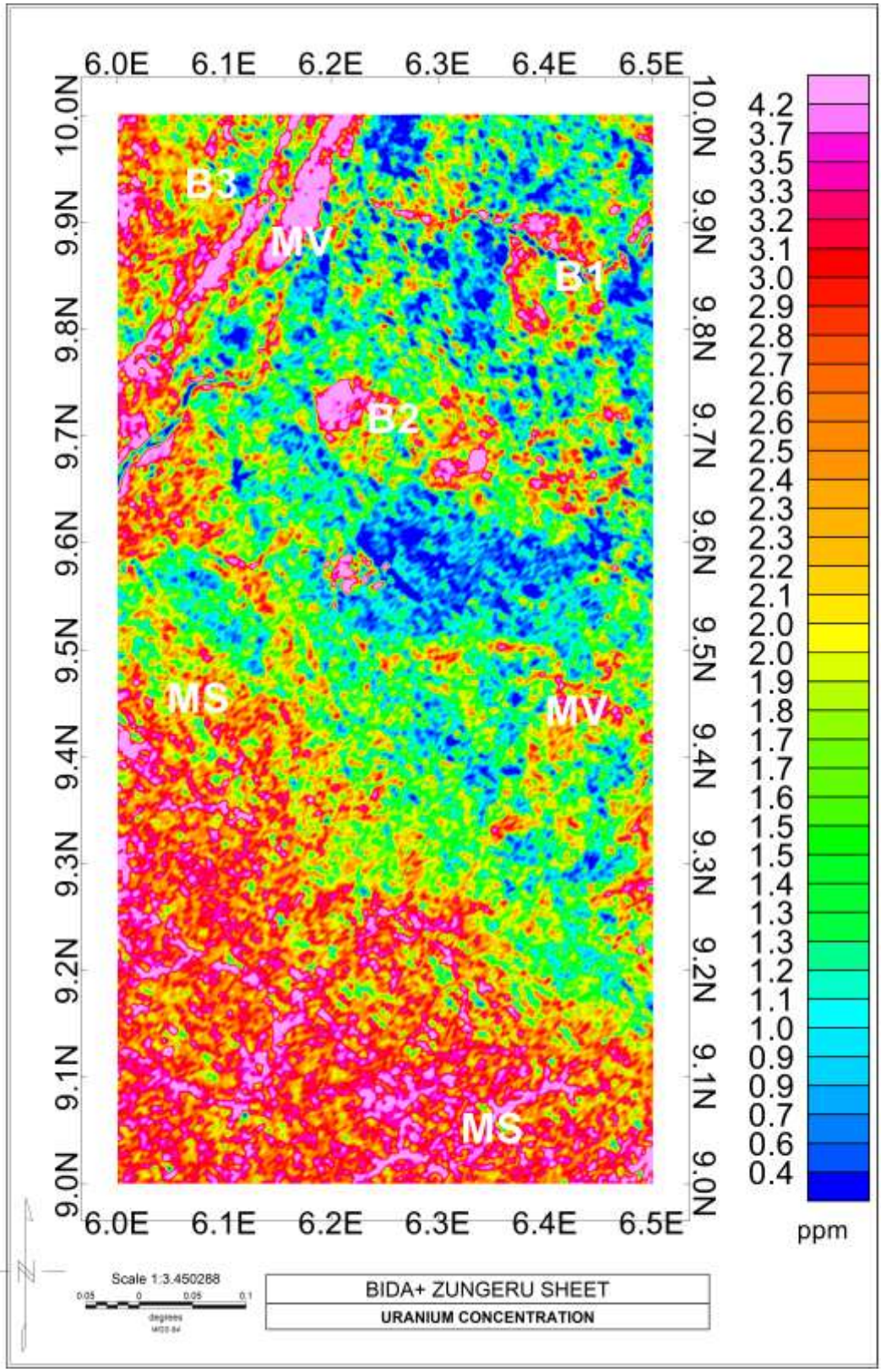

Figure 4.10: Uranium concentration map of the radiometric data of Bida and Zungeru

4.11 Delineating Mineralised Structure

Alteration from the contact between cretaceous sediment, metasediments and intrusions within the belt type granite and schist and have change and destroy the chemical composition of majority of the rocks within the study area, which can be seen on both the radiometric and magnetic datasets. The various changes in concentration of potassium and thorium within metasediments in the regions of MV B1,B2 ,B3 and below FUT main campus are clear evidence of hydrothermal alterations as observed by Griffis *et al.* (2002) that mafic volcanic rocks generally lack potassium bearing minerals and K enrichment are not accompanied by Th during hydrothermal alterations. In the magnetic analysis such as the analytical signal, the first vertical derivative revealed a contact between metasediment and sedimentary formation are clearly demarcated by shear zones, faults, fractures and low magnetic susceptibility (Figure 4.5). These are due to volcanic activities that accompanied by rock deformation and metamorphism especially within the brittle shear zones (Griffis *et.al* 2002).

The regions that are hydrothermally altered are possible targets that control gold mineralization of the study area specific regions delineated and mapped include F1, F2, F4, F5, F6, F7, F8. Below B2, they are strategically located within the mylonite and schist deposit at the NW corner of the area, below B2 and B1 within the metasediment, (MS) and below FUT main campus around Sabon-Dagga, Kakagi, Babo Shiri, Sunbwagi, Mikwegi and Minkwoigi etc within the migmatite at the lower eastern end.

4.12 Ratio Maps of K/Th, U/K and Th/U

Grid math and stitching of the channel were used to maximize contrast and mark subtle features in the data. The degree to which the source materials of regolith are weathered or leached were asses with the used of Th channel and ratio channels (K/Th and Th/U).

According to Wilford *et al.* (1997), Potassium K response is associated with easily weathered minerals, whereas thorium and uranium are usually related with residual clay, oxides and accessory minerals. Figure 4.11 represents K/Th concentration which indicates some lithology contact and promote alteration signatures. The increase in K content and decrease in K/Th ratio observed for the intrusive belt granitoid and mafic meta-volcanic (Figure 4.8 and Figure 4.11) shows hydrothermal alterations. These occur as a result of the mafic volcanic rocks generally lack K- bearing minerals and K enrichments are not accompanied by the Th during hydrothermal alteration processes (Dickson and Scott, 1997). The K/Th ratio map shows that high content of potassium in the red color implies weak content of thorium and vice versa.

Ostrovskiy (1975), discovered that the reduction in thorium with the increase in potassium occur at the shear contact zone between meta-sediment, meta-volcanic and cretaceous sediment which were also observed at north east, north west and upper region part of south east (Figure 4.11) of the study area shows the accumulation of various deposited of ore. On the other hand, a number of mineralization of gold districts demonstrate a rise in potassium and thorium like intrusion of the belt type granitoid in the north east direction within the meta-sediment implies that thorium was mobilized during the hydrothermal activities.

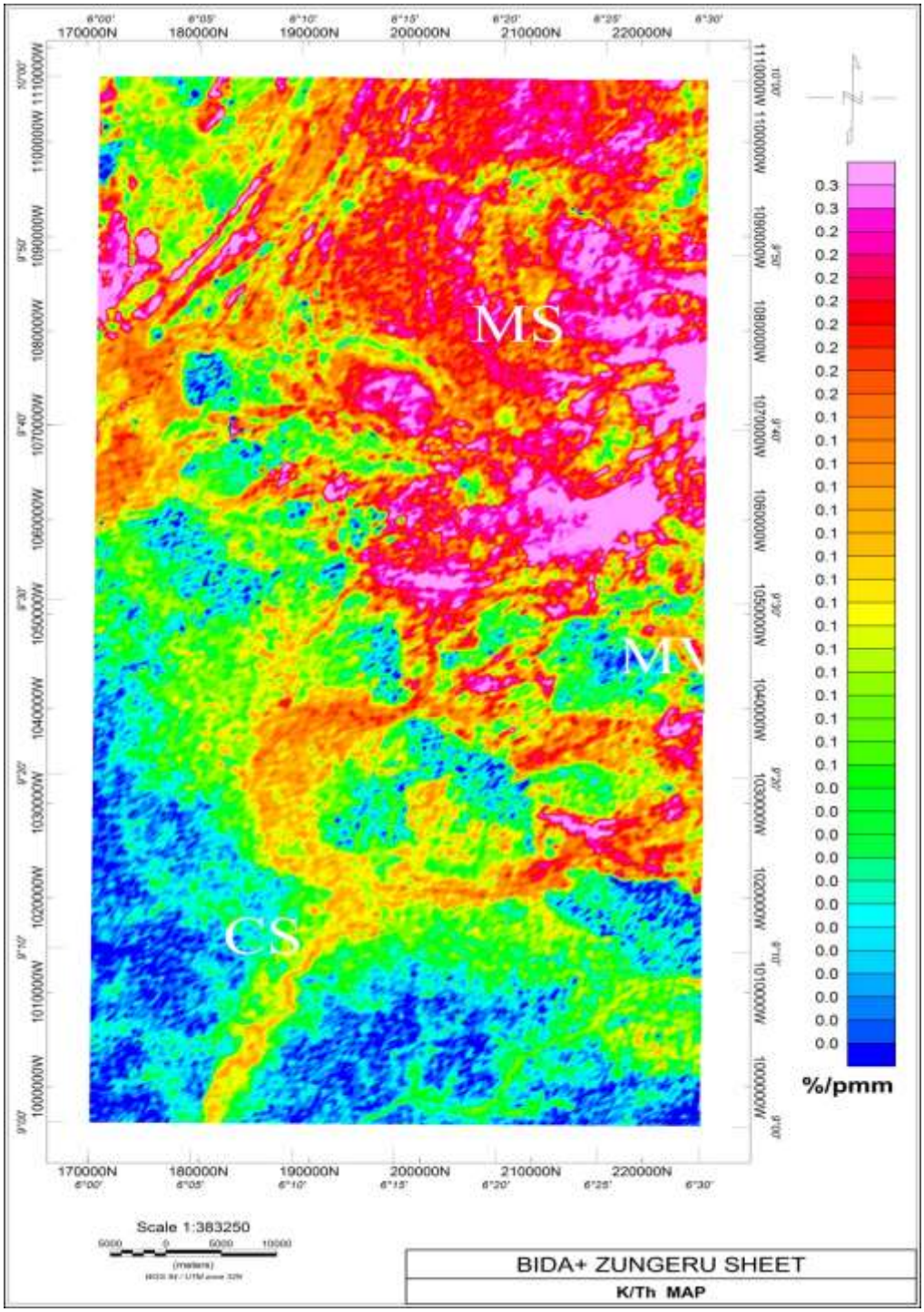

Figure 4.11: A ratio potassium and thorium (K/Th)

The U/K ratio map was used to determine areas where contents of uranium are relatively strong. A number of the uranium U intensities are associated with zone of mineralisation of gold delineated in contact with and within both meta-sediment and cretaceous sediment. The high uranium concentration was recorded at south west and south east of Bida region where rubbles material (Alluvium) deposited by running water was identified

when correlate with the geology map of the study area. The fairly low potassium content was also recorded at this region.

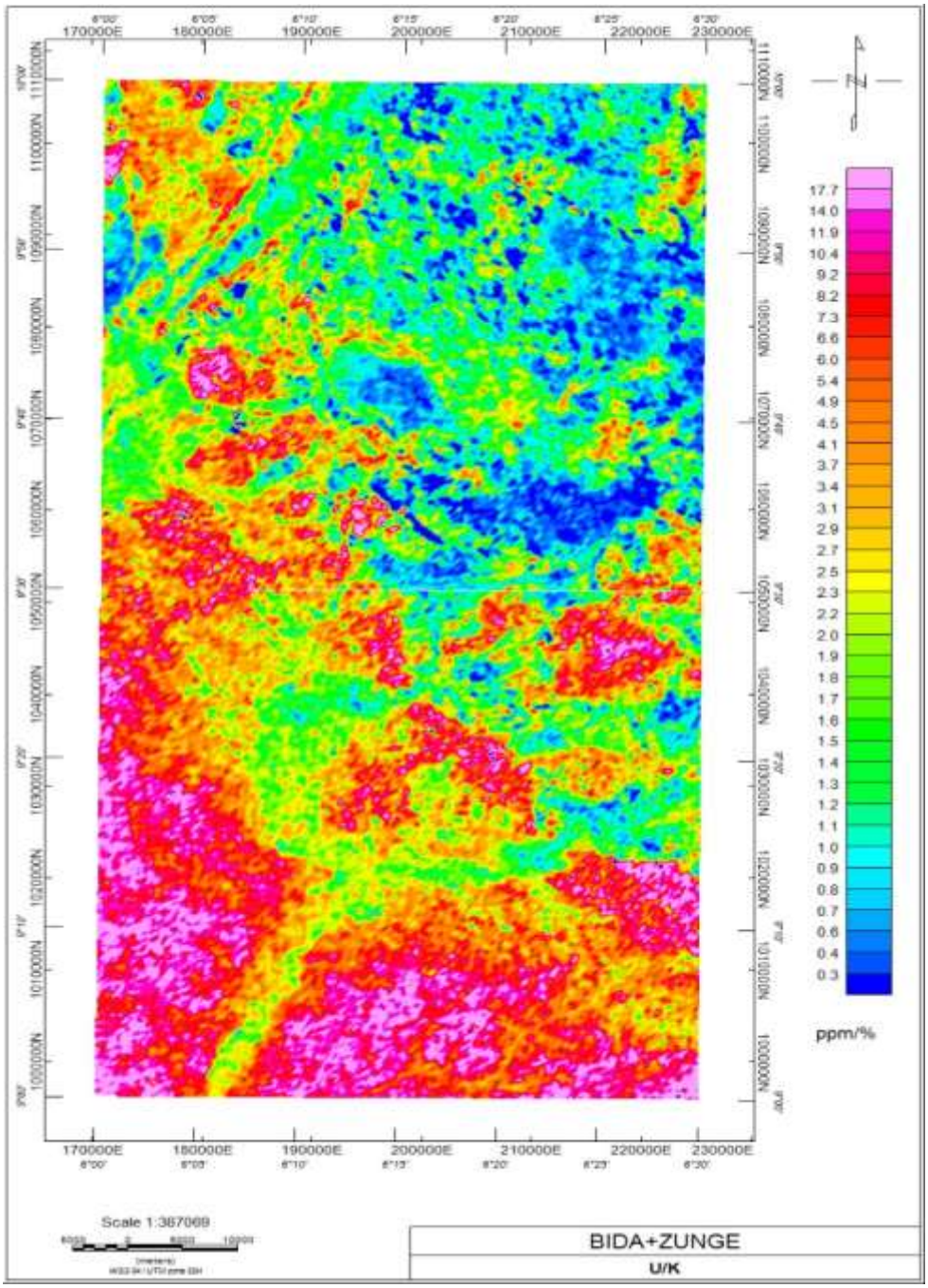

Figure 4.12: A Ratio of uranium and potassium (U/K) of Bida and Zungeru

High K/Th (Figure 4.11) and low U/K (Figure 4.12) over potassic formations within the concession are likely to be characterised with slightly weathered and high leached soils respectively. The ratio image of Th/U (Figure 4.13) shows that almost of the study area is dominated by high thorium Th concentration. The Th/U map mark Th alteration zone

reflecting coincidentally increase Th and lowered Uranium U or potassium K. The Zungeru region (meta-sediment) are seen to record high Thorium concentration and fairly high at south west (cretaceous sediment) at Bida region with a trace of Uranium concentration.

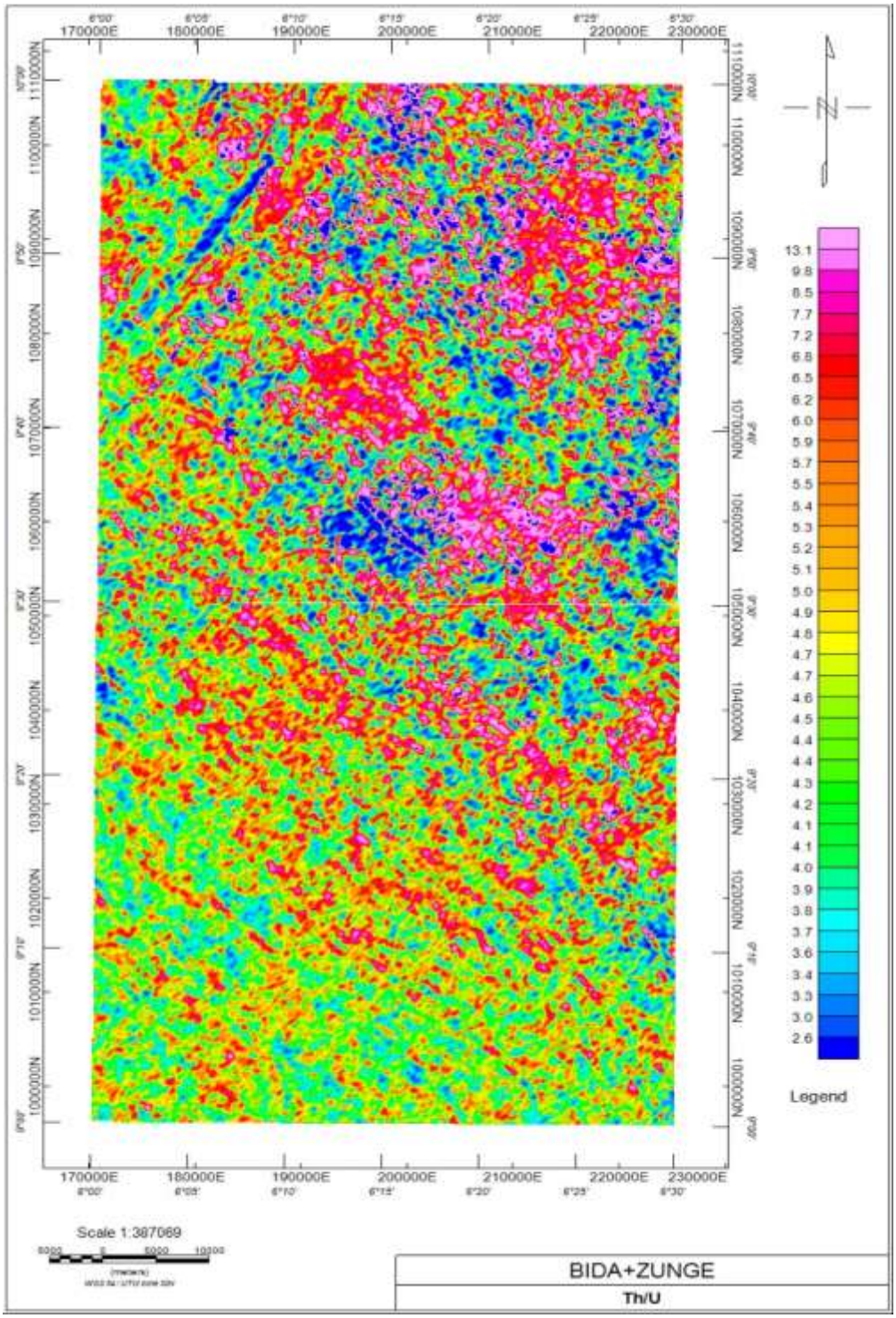

Figure 4.13: A ratio map of thorium and uranium of Bida and Zungeru

4.13 Ternary Map

Representing uranium, thorium and potassium with blue, green and red coloration respectively the ternary map was produced to represent individual concentration of the gamma radiation and corresponds to slight variations in their relative amount. The map shows a sharp contrast between the geological formations identified within the study area. The high relationship due to the fact that the formations such as biotite, granite, the cretaceous sediment and biotite gnesis have potassium contact. The regions containing the amphibolites, mylonite and magmatite shows darker that the neighboring formations indicating weak content in potassium, thorium and uranium. The white area in the composite map are indication of strong contents in K, Th and U, while cyanide indicate area of strong potassium and thorium but weak uranium and yellow indicates area of strong potassium and uranium but weak thorium content. The magenta shows area of strong thorium and uranium but low potassium content. Blues and dark blue regions marked the study areas most of which are within the contact and fault regions, they are related to the belt type granite also at the eastern corner between 9˚45- 10˚0N and below the spherical bodies B1, B2 equally within B3 and above MV indicating low intensity of uranium (Figure 4.14) but high potassium and thorium. The high uranium within these regions suggests young granitoid intrusions accompanied by low magnetic intensity. Below the FUT main campus region excessive weathering must have used up, most of the uranium content this informs the magenta coloration observes just below latitude 9˚30N (Minkwoigi, Kakaki, Sunbwagi, Sabon-dagga and Bobo Shiri). It was observed by Hoover and Pierce (1990) that airborne gamma ray surveying marks of deposit of gold were chargeable with potassium being most dependable guide regions hosting gold within quartz vein, hydrothermal alteration of causative body can provide reliable links. In this research potassium is related to most favorable host rocks. Low potassium anomalies are

observed along the contacts between the cretaceous sediments and the metasediments trending NW-SE and within the mylonite at the northwestern corner of the study area. Hydrothermal zone, faults, veins and foliation host the mineralisation of gold within the study area. The contacts zone depicts low potassium and high thorium and uranium (Figure 4.14) respectively. The weak potassium anomaly could indicate potassic alteration associated with an increase fluid entry that migrates through low pressure and high faulted zones within this area. (Dickson and Scolt 1997)

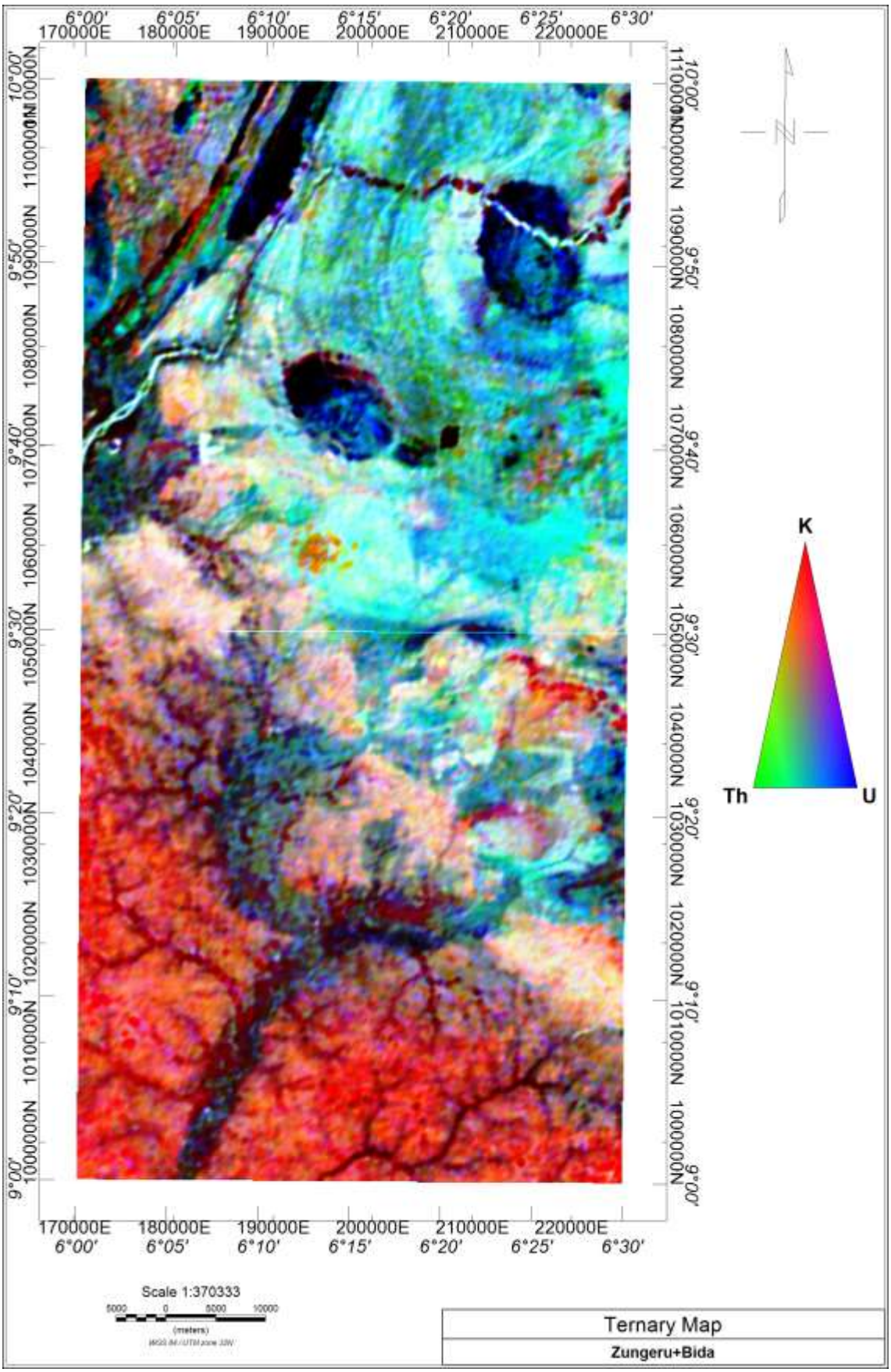

Figure 4.14: Ternary map of the study area of Bida and Zungeru

4.14 Summary of the Result

Both aeromagnetic and radiometric data of Zungeru and Bida areas were interpreted to delineated regions of gold mineralization and other associated minerals. An area of 55 Km ×110 Km square was subjected to various analytical and visual analysis such as horizontal derivative, vertical derivative, analytical signal, Euler deconvolution and Centre exploration targeting (CET) results of these shows that the total magnetic intensity map figure 4.1 comprises of both positive and negative anomalies. The negative anomalies are mostly within the cretaceous sediment with some isolated lows within the metasediments. Magnetic susceptibility ranges from -119nT to 147.9nT. Variations in susceptibility are due to lateral variation in rock susceptibility and the susceptibility of the basement depth of barrier and remnant magnetisation.

The analytical signal map obtains from the horizontal derivatives in x, y and z directions depicts the amplitude response of the magnetic susceptibility range from 0.010m to 0.122m within the sedimentary formation and 0.134m to 0.493m within the metasediment specify of major anomalies were clearly observed and anomalies were clearly delineated above the causative bodies.

The first vertical derivatives maps help us to place features such as lineaments both on high regions of susceptibility (in red) and low regions of susceptibility (in blue), geology contacts (yellow), folds (bold yellow) all across the field prominently at the North-Western corner of the study area. These are sets of linear structure that trend NE-SW, located within the mylonites and mylonites interlayer by amphibolites which are the belt-type meta-sediments. Equally worth mentioning are sets of lineaments (in blue) trend E-W all across the mid region of the study area. Where majority of volcanic activities must have been recorded. The prominent feature clearly unavoidable are the spherically shaped

intrusive bodies marked as B1and B2 at the upper part of the study area with low susceptibility. All the folds and the contact are located between the cretaceous sediment and metasediment basement region.

The Centre Exploration Targeting (CET) method delineating and mapped lineament and structures automatically. These lineaments and structures correlate with what were observed in first vertical derivative maps.

Euler Deconvolution method shows that majority of these structures are situated between 30 to 300meters all across the field within the metasediment. Generally, structures with depth estimate within 30 to 160 meters dominate the field most especially around Sabon-Dagga, Kakaki, Sunbwagi, Bobo Shiri, Minkwegi and Minkwiogi.

The Potassium concentration map (Figure.4.8) depicts high anomaly signals at the upper north and eastern part of the study area, worthy of note is another high anomaly notice within the Alluvium deposits at the lower Bida sheet. This coincides with the channel of tribute river-wuya, where erosion has exposed the basement. Anomalous signatures were observed within the cretaceous sediments has relatively low potassium K concentration around the western end and southern part of the study area.

The thorium concentration map (Figure.4.9) illustrates clearly lithology distinctions. A clear demarcation between the cretaceous sediment and metasediment is clearly shown. Fairly high anomalies represent the mylonite, amphibolites and granite at the upper north western corner of the study area. High concentration thorium on bodies defines as B1, B2 and B3 were observed, but very low concentration was observed just below B2.

The uranium concentration map (Figure.4.10) also depicts a demarcation between the cretaceous sediment and metasediment. Fairly high anomalies represent the mylonite,

amphibolites and granite at the upper north western corner of the study area. A relatively low uranium concentration on bodies defines as B1, B2 and B3 were observed but very low concentration was observed just below B2.

The ratio maps such as Th/K, U/K and Th/U were generated to get rids of the lithological variations caused by differences in the water content in soil, non-planar source geometry and errors related with altitude. The K/Th map also define hydrothermal alteration zone around Sabon-Daga, Kakagi, Sunbwagi, Minkwegi and Minkwoigi show highly weathered structures with low potassium concentration. High relatively concentration of uranium was also observed in U/Th and U/K ratio maps.

Ternary map (Figure.4.14) obtains from concentration map of potassium, thorium and uranium represents blue, green and red coloration respectively. This map shows a sharp contrast between geological formations between the cretaceous sediment and metasediment identify within the study area. The white area in the composite map are indication of strong contents in K, Th and U, while cyanide indicate area of strong potassium and thorium but weak uranium and yellow indicates area of strong potassium and uranium but weak thorium content. The magenta shows area of strong thorium and uranium but low potassium content. Blues and dark blue regions marked the study areas most of which are within the contact and fault regions, they are related to the belt type granite also at the eastern corner between 9˚45- 10˚0N and below the spherical bodies B1, B2 equally within B3 and above MV indicating low intensity of uranium (Figure 4.14) but high potassium and thorium. The high uranium within these regions suggests young granitoid intrusions accompanied by low magnetic intensity. Below the FUT main campus region excessive weathering must have used up, most of the uranium content this informs the magenta coloration observes just below latitude 9˚30N (Minkwoigi, Kakaki,

Sunbwagi, Sabon-dagga and Bobo Shiri) are the hydrothermal alteration zone. Low potassium anomalies are observed along the contacts between the cretaceous sediments and the metasediments trending NW-SE and within the mylonite at the northwestern corner of the study area.

The coordinate of these major structures shows degree of mineralization has been mapped on Centre Exploration Targeting Map (figure 4.7) most interestingly is between longitude 6˚20E to 6˚30E and latitude 9˚10N to 9˚30N and which coincide with hydrothermal alteration zone identified on ternary map. Also, longitude 6˚00E and latitude 9˚45N, longitude 6˚12E and latitude 10˚00N, longitude 6˚20E and latitude 9˚50N at the Zungeru part of the study area.

CHAPTER FIVE

5.0 CONCLUSION AND RECOMMENDATIONS

5.1 Conclusion

The examinations of the geophysical datasets in the study area provide detailed information into the structural construction. Two major geological units exhibit the study area cretaceous sediment and the meta-sediments. The major feature identify within the Cretaceous sediment are the folds' majority of which are located within their contacts.

The mineralisation of gold is strongly characterised with quartz stock work rocks sourced predominately in granite. The gold can be found within this vein and in the adjacent, highly deformed host rock located around Minkwoigi, Sunbwagi, Kakagi, Sabon dagga and Bobo shiri towns. The deformation seems to comprises principally of pebbly schist, amphibolites along fine grained and magnetite. It happens in very fine grains, strongly characterized with pyrite and seems to have been introduced along with carbonate and Sulphur which post-date the previous deformation (silica, sericite and iron oxides) Griffis *et.al*., (2002).

The airborne radiometric showed a mobilization of the immobile thorium Th concentration and this also indicated hydrothermally altered zones. The increase in potassium concentration and decrease in K/Th relation observed from radiometric interpretation are very pinpointing of hydrothermal activities within the study area.

In conclusion, mineral deposits were identified. This reveals a major structural features located just below FUTMinna around Minkwoigi, Sunbwagi, Kakagi, Sabon Dagga and Bobo Shiri town that include shear zone, faults, shear and fault intersections and fractures systems magnetic anomalies that mainly trend E-W and NW-SE direction. This may be attribute of hydrothermal activity where hydrothermal fluids move to low pressured

regions where these faults occur and generated heat destroy the magnetization within the causative rocks hence low magnetic intensities are related with the delineated faults. The K/Th map also reveals this area with low potassium concentration but high thorium concentration.

5.2 Recommendations

From the foreseen results an appropriate ground suiting using electrical or gravity method is recommended at those locations delineated, taking the coordinates into reference, this is to actualise the economic viability of the deposits.

REFERENCES

Adetona, A. A., & Mallam, A. (2013). Estimating the thickness of sedimentation within lower Benue Basin and Upper Anambra Basin, Nigerian. Using both spectral depth determination and source parameter imaging. *ISBN Geophysics,* Vol. 2013,1-10 Article ID 124706,

Afegbua, U. K., Yakubu, T. A., Tsalha, M. S., Ologun, C.O., Oluwadare, T.S., Duncan, D. Uwazuruonye, J., Okwunma, G., Ekweuzoh, P., Enang, M., & Agoro O. A. (2017). Geological. Geophysical and Seismological Investigation for siting of Seismic Stations in Minna and Abakaliki, Nigeria for Data Reliability. *British Journal of Applied Science & Technology pg 6*

Airborne-Radiometric Data Processing and Interpretation Chapter iv pg 142

Ajaikaiye, D.E., Hall, D.H., Ashiekaa, J. A., & Udensi E. E. (1991). Magnetic anomalies in the Nigerian continental mass based on aeromagnetic surveys. *Tectonophysics*, 192: 211-230.

Ajibade, A. C. (1976). Provisional classification and correlation of the schist belts of Northwestern Nigeria. In Kogbe, C.A., Ed., Geology of Nigeria, Elizabethan Pub.co., Lagos, 88-90

Alabi A.A. (2011). Geology and environmental impact assessment and benefit of granite Rocks of Minna Area, Northwest Nigeria. *Ethiopian Journal of Environmental Studies and Management*, 4(4), 39-45

Anabana, S.E. and Ajakaiye, D. E. (1987). *Evidence of tectonic control of mineralization in Nigeria from lineament density analysis. International Journal Remote Sensing 8(10), 1445-1453*

Bello A. (2012). Use of Electrical Resistivity Technique to Delineate Gold Deposit site in Minna, Niger State Nigeria. *International Journal of Science and Technology. 2(8) pp 596-599*

Bhattacharyya, B. K. & Leu, L. K. (1977) Spectral analysis of gravity and magnetic anomalies due to rectangular prismatic bodies, *Geophysics*, 42, 41–50.

Bhattacharyya, B., & Leu, L. K. (1975). Analysis of magnetic anomalies over Yellowstone National Park: mapping of Curie points isothermal surface for geothermal reconnaissance. *Journal of Geophysical Research, 80*(32), 4461-4465.

Boadi, B., David D. W., & Kwasi P. (2013). Geological and structural interpretation of the konongo area of the Ashanti gold belt of Ghana from Aeromagnetic and radiometric data. *International Research Journal of Geology and Mining. 3(3) pp. 124-135 April 2013 Available online* http://www.interesjournals.org/ IRJGM

Buser H. (1966) *Paleo structures of Nigeria and adjacent countries*. Scheizerbartsche veragsbuchandlung, Stuttgart.

Clark, D.A. & Emerson, D.W. (1991) Notes on Rock Magnetization Characteristics in Applied Geophysical Studies. *Exploration Geophysics*, 22, 547-555. https://doi.org/10.1071/EG991547

Darnley, A. G., & Ford, K. L. (1989) Regional airborne gamma-ray syrvey: A review; in "Proceedings of Exploration 87: *Third Decennial International Conference on Geophysical and Geochemical Exploration for Minerals and Ground Water",* Geol. Surv. of Canada, Special Vol. 3, 960 p

David, I., & Marius, N., U. (2013). Interpretation of Aeromagnetic anomalies over some parts of lower Benue trough using spectral analysis techniques *International Journal of Scientific & Technology Research 2(8) 153-165*

Debeglia, N., & Corpel, J. (1997). Automatic 3-D interpretation of potential field data using analytical signal derivative: *Geophysics*, 6, 87-96,

Dickson, B. L., & Scott, K. M. (1997). Interpretation of Aerial Gamma-Ray Surveys-Adding the Geochemical Factors *Journal of Australian Geology and Geophysics*, 17, 187-200

Eze, E., Nwannediya, D., Femi, O., Abdullahi, B., & Olarenwaju, A. E. (2019). FUTMinna, *Book of Speeches 28th Convocation Ceremony*. Page 12.

Geosoft Inc., (1996): Oasis Montaj Version 6.3 User Guide, Geosoft Incorporated, Toronto

Geosoft Inc., (2010): Oasis Montaj Version 6.3 User Guide, Geosoft Incorporated, Toronto

Grant, F. S., & Dodds, J. (1972) MAGMAP Fast Fourier Transform processing system development notes, Paterson Grant and Watson Limited. Grid Exchange File, Geosoft Inc, 1999,

Grauch, V. J. S., Jeffrey D, Phillips, D. B., Hoover, J. A., Pitkin, K., Eric, L., & Anne, M. (1993). Materials provided at the workshop "Geophysical map interpretation on the PC" Convened April 21-23, Chapter 3, Page 3-7

Griffis, R. J. (1998). Explanatory Notes – Geological interpretation of geophysical data from southwestern Ghana. Minerals Commission.

Griffis, R. J., Barning K, Ageno F. L., & Akosah, F. K. (2002). *Gold deposits of Ghana*. Minerals Commission Report.

Hobart, M. K. (2005). Relative abundance percentages from Ronov and Yaroshevsky; *Chemical Composition of the Earth's Crust*; American Geophysical Union Monograph Number 13, Chapter 50, 1969.

Hoover, D. B., Heran, W. D. and Hill, P. L. (1992). The Geophysical Expression of Selected Mineral Deposit Models. U.S. Geological Survey Open-File report 92–557, pp. 129

Hubbard, F. H. (1975) Precambrian crustal development in western Nigeria: indications from Iwo Region. *Geology Society of America Bulletin* 86:548-554

Idris-Nda., A. Abubakar, S. I, Waziri, S. H., Dadi, M.I., & Jimada, A. M. (2015). Groundwater development in a mixed geological terrain: a case study of Niger State, Central Nigeria. WIT Transactions on Econlogy and The Environment, Vol 196, 78-87 © 2015 WIT Press www.witpress.com, ISSN 1743-3541 (on-line)

International Atomic Energy Agency. (2003). *Guidelines for radioelement mapping using gamma ray spectrometry data: Also, as open access e-book.* Vienna:

John, U. M. & Udensi, E. E. (2013). Lineaments study aeromagnetic data over parts of southern Bida basin, Nigeria and the surrounding basement rocks. *International Journal of Basic and Applied Science2(1) (2013) pg 115 124©Science Publishing Corporation.www.sciencepubcob. com/ index. php/IJBAS.*

John, U. M., Udensi, E. E., Olasehinde, P. I, Mohammed, D. A., & Lawal, K. M. (2013). Geothermal and radioactive heat studies of parts of southern Bida basin, Nigeria and the surrounding basement rocks. *International Journal of Basic and Applied Science* 2(1) 2013 125-139

Jude, E. S., Peter O., Appollonia A. O., & Ipoola, O. (2017). Investigation of Hydrogeological Structure of Paiko Region, North-Central Using Integrated Geophysical and Remote Sensing Techniques.*Geosciences*.7(122)1-17

Kovesi, P. D. (1996). MATLAB code for calculating phase congruency and phase symmetry/asymmetry, http://www.cs.uwa.edu.au/pk/Research/research.html.

Kuforijimi, O., & Chibuzor, G. C (2018). Analysis of Geothermal Heat Flow Potentiality of Upper Bida Basin Nigeria Using Aeromagnetic Data. *International Journal of Applied Science* 5(2) 1-7

Lam L., Lee, S. W & Suen, C. S. (1992). "Thinning Methodologies -A Comprehensive Survey", IEEE Transactions on Pattern Analysis and Machine Intelligence, Vol. 14, No. 9, Sept. 1992, pp. 869-885

McCURRY, P. (1976). *The geology of Precambrian to lower Paleozoic rocks of northern Nigeria-a review*

McDonough, William F. (1999) *Earth's core In Encyclopedia of Geochemistry (Encyclopedia of Earth Sciences series*) (Ed. Marshall, Clare P. & Fair bridge, Rhodes W), Spriger.151-155.

Mendonca, C. A., & Silva, J. B. C. (1993). A stable truncated series approximation of the reduction-to-the pole operator: *Geophysics*, (58) 1084–1090.

Milsom, J. (2003). *Field geophysics*. 3rd Edition. John Wiley and Sons Ltd, London. 232pp

Mittlefehldt & David M. (1999) Potassium. In: Encyclopedia of Earth Sciences Series (Ed. Marshall, Clare P. & Fairbridge. Rhodes W.) Springer. 522,

Nabighian, M. N. (1972). The analytical signal of two-dimensional magnetic bodies with polygonal cross –section: Its properties and use for automated anomaly interpretation: *Geophysics*, 37, 507-517

Ngama, J., & Akanbi, E. S. (2017). Qualitative Interpretation of Recently Acquired Aeromagnetic Data of Naraguta Area, North Central Nigeria using Analytical Signal Method. *Journal of Geography, Environmental and Earth Science International 11(3): 1-14, 2017; Article no. JGEESI.35529 ISSN: 2454-7352*

Nigeria Geological Survey Agency, (2009). Geological Map of Nigeria

Nwagbara, J. O., Nwugha, V. N., Okorie, J. O., Nokereke, C., & Chinemelu, E. S. (2012) Geophysical estimate of depth of some anomalous geologic features in parts of lower Benue trough. *International Journal of Emerging trends in Engineering and Development* 4(2012), 517-519

Nwosu O. B. (2014). Determination of Magnetic Basement Depth over Parts of Middle Benue Trough by Source Parameter Imaging (SPI) Technique Using HRAM. *International Journal of Scientific & Technology Research Volume 3, issue 1, ISSN 2277-8616 pp 262-271*

Obaje, N. G. (2009). *Geology and Mineral Resources of Nigeria*, London: Springer Dordrecht Heidelberg, Pp5-14,

Oke, I. O., Adetona, A. A., & Oke, A. (2018). Interpretation of high-resolution aeromagnetic data to determine sedimentary thickness over part of Bida Basin, North Central Nigeria. *Journal of Geology and Mining Research. 10(6), pp. 72-80,*

Ostrovskiy, E. Y. (1975). Antagonism of radioactive elements in wall rock alteration fields and its use in aerogamma spectrometric prospecting: *International Geology Review*, 17(A) p. 461-468.

Phillips, J. D. (2005). Can we estimate total magnetization directions from aeromagnetic data using Helbig's integrals Earth, Planets and Space, 57, 681–689

Pierre Keating (1995). Error estimation and optimization of gravity survey. Geophysical Prospecting 43(4), 1365-2478.

Roest, W. R., Verhoef, J., & Pilkington, M. (1992). Magnetic interpretation using 3-D analytical signal: *Geophysics,* 57,116-125.

Silva, A. M, Pires, A. C., McCafferty, A., Moraes, R., & Xia, H. (2003). Application of airborne geophysical data to mineral exploration in the uneven exposed terrains of the Rio Das Velhas greenstone belt. *Revista Brasileira de Geosciences*, 33(2), 17-28.

Udensi, E. E., Osazuwa, I. B., & Daniyan M. A. (2003). Trend analysis of the total magnetic field over Bida basin, Nigeria. Federal University Technology, Minna and Ahmadu Bello University, Zaria.

Wilford, J. R., Bierwirth, P. N. & Craig, M.A. (1997). Application of airborne gamma-ray spectrometry in soil/regolith mapping and applied geomorphology. AGSO *Journal of Australian Geology and Geophysics* 17 (2): 201-216.